Table 1. Variant priority scheme after exome sequencing[a]

	NEXTGENE	II-2	MAQ (SEATTLESEQ)
Total variants called	22,176	—	58,081
Chr X	3441	—	4383
Unknown SNP variants (dbSNP131, 1000 genomes)	910	—	882
Overlap of NEXTGENE and MAQ	—	169	—
NS/SS	—	17	—
Except for variants at segmental duplications	—	15	—

NS, non-synonymous; SNP, single-nucleotide polymorphism; SS, splice site (±2).
[a]MAQ was annotated with SEATTLESEQ ANNOTATION. The annotation includes gene names, dbSNP rs ID, and SNP functions (e.g. missense), protein positions and amino acid changes.

cell for II-2 (Illumina). Image analyses and base calling were performed using sequence control software real-time analysis and OFFLINE BASECALLER software v1.8.0 (Illumina). Reads were aligned to the human reference genome (UCSC hg19, NCBI build 37.1).

Mapping strategy and variant annotation

The quality-controlled (Path Filter) reads were mapped to the human reference genome (UCSC hg19, NCBI build 37.1), using mapping and assembly with quality (MAQ) and NEXTGENE software v2.0 (SoftGenetics, State College, PA). Single-nucleotide polymorphisms in MAQ-passed reads were annotated using the SEATTLESEQ ANNOTATION website (http://gvs.gs.washington.edu/SeattleSeqAnnotation/).

Priority scheme and capillary sequencing

Called variants found by each informatics method were filtered in terms of location on chromosome X, unregistered variants (excluding registered dbSNP131 and 1000 Genomes), overlapping variants called in common by NEXTGENE and MAQ, and non-synonymous changes and splice-site mutations (±2 bp from exon–intron junctions) (Table 1). The variants were confirmed as true positives by Sanger sequencing of polymerase chain reaction (PCR) products amplified using genomic DNA as a template, except for variants within genes at segmental duplications. Sanger sequencing was performed on an ABI3500xl or ABI3100 autosequencer (Life Technologies, Carlsbad, CA). Sequencing data were analyzed using SEQUENCHER software (Gene Codes Corporation, Ann Arbor, MI).

Reverse transcription-PCR

Total RNA was isolated from EBV-transformed lymphoblastoid cell line (EBV-LCL) derived from II-2 and healthy control subjects using the RNeasy Plus Mini Kit (QIAGEN). Five micrograms of total cellular RNA was used for reverse transcription with the Super Script III First-Strand Synthesis System (Life Technologies). Two microliters of synthesized complementary DNA was used for PCR with the following primers: ex17-F (5′-CTACCATCACCCACTGAGTC-3′) and ex19-R (5′-TGAGACATATCCCCGGCAG-3′). Amplified PCR products were electrophoresed in agarose gels, purified from gels using the QIAquick Gel Extraction Kit (QIAGEN), cloned into pCR4-TOPO vector (Life Technologies) and sequenced.

X-chromosome inactivation assay

The human androgen receptor (HUMARA) assay was performed as previously reported (9). Genomic DNA of II-2 was digested at 37°C for 18 h with two methylation-sensitive enzymes, *Hpa*II and *Hha*I. PCR was performed using digested and undigested DNA with HUMARA primers (FAM-labeled ARf: 5′-TCCAGAATCTGTTCCAGAGCGTGC-3′; ARr: 5′-CTCTACGATGGGCTTGGGGAGAAC-3′). DNA fragment analysis was performed on an ABI3130xl autosequencer (Life Technologies). Fragment data were analyzed with GENEMAPPERT SOFTWARE version 4.1 (Life Technologies).

Results

Exome sequencing

Because this disorder was assumed to be an 'X-linked recessive' disorder based on the initial pedigree information, we focused on the X chromosome. Approximately 4.5 Gb of sequence data were generated, 87.3% of which was mapped to the human reference genome (UCSC hg19, NCBI build 37.1). MAQ was able to align 53,242,972 reads to the whole genome.

Two informatics methods identified 17 potential pathogenic changes (15 missense mutations, 1 nonsense mutation, and 1 splice-site mutation) (Table 1). The nonsense mutation was a false positive and all 13 missense mutations were inconsistent with the phenotype (no co-segregation). The mutation c.2388+1G>C was identified at the splice-acceptor site of intron 17 in *OFD1*, heterozygously in II-2, and hemizygously in III-5, but was absent in II-3, III-3, and III-6 (Fig. 3a) as well as 93 normal female controls (0/186 alleles).

RT-PCR, direct sequencing

To examine the mutational effects of c.2388+1G>C, reverse transcriptase-polymerase chain reaction (RT-PCR) was performed. Only a 239-bp PCR product (wild-type allele) was observed in healthy control individuals (Fig. 3b). By contrast, a longer 1364-bp product was detected in II-2. Sequencing of the 1364-bp product revealed that a 1125-bp sequence of intron 17 was retained, producing a premature stop codon at amino acid position 796 (Fig. 3b). These data indicate

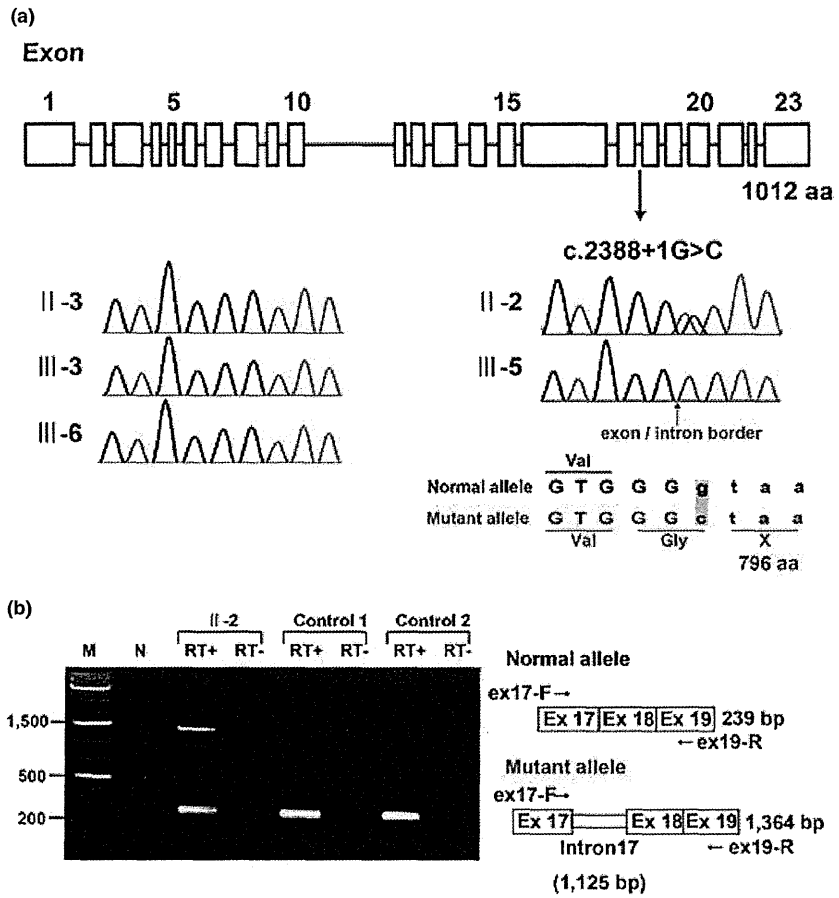

Fig. 3. (a) Gene structure of *OFD1* with the mutation (c.2388+1G>C) (upper). Electropherograms of the family members. Wild-type sequences are seen in II-3, III-3 and III-6. Heterozygous and hemizygous mutations are observed in II-2 and III-5, respectively. (b) Reverse transcriptase-polymerase chain reaction analysis showing both 239-bp and 1364-bp products in II-2, and only 239-bp products in two normal female controls. The 239-bp product is normal and the 1364-bp product is aberrant.

that the c.2388+1G>C mutation in *OFD1* is most likely the causal mutation in this family.

X-chromosome inactivation assay

X-chromosome inactivation patterns was random patterns in II-2 available for this study (ratio > 38:62).

Discussion

Exome sequencing detected a single-base substitution (c.2388+1G>C) in *OFD1*, resulting in an error in splicing of intron 17 and a premature stop codon at amino acid position 796, in an affected male (III-5) and a carrier female (II-2) in this family with an 'unclassified' X-linked lethal congenital malformation syndrome. II-4 and III-1, who had strikingly similar clinical manifestations to III-5, are likely to have had the same *OFD1* mutation as III-5, although their DNA was not available. Through reassessment of clinical features of the family, the three affected males shared facial, oral, and digital malformations characteristic of OFD1 (4). Additionally, they exhibited more severe complications in various systems including congenital heart defects, genitourinary malformations, and ophthalmological abnormalities. II-2 was also found to have subtle features of OFD1 (accessory frenulae and irregular teeth). Thus, we have concluded that the 'unclassified' X-linked lethal congenital malformation syndrome in this family was clinically compatible with OFD1.

An *OFD1* mutation (c.2123_2126dupAAGA in exon 16, p.Asn711Lysfs*3) was also detected in a family with an X-linked recessive mental retardation syndrome (10). Nine affected males had macrocephaly and severe mental or developmental retardation, and suffered from recurrent respiratory tract infections leading to early death in eight. Only an 11-year-old boy survived with severe mental retardation (IQ 20), obesity, and brachydactyly. His younger brother had postaxial polydactyly. No cognitive, oral, facial, digital, or renal abnormalities were detected in heterozygous carrier females in that family. The patients were later classified into an infantile lethal variant of Simpson-Golabi-Behmel syndrome (type 2) (SGBS2, OMIM #300209), which had consisted of only one family,

genetically mapped to Xp22, including four maternally related affected males with hydrops at birth, craniofacial anomalies (macrocephaly, low-set posteriorly angulated ears, hypertelorism, short and broad nose with anteverted nares, large mouth with thin upper vermilion border, prominent philtrum, high-arched or cleft palate, and short neck), redundant skin, hypoplastic nails, skeletal defects involving upper and lower limbs, gastrointestinal and genitourinary anomalies, hypotonia and neurological impairment, and early death within the first 8 weeks (11, 12). Other *OFD1* mutations were detected in two families with Joubert syndrome-10 (JBTS10, OMIM #213300) (13). A mutation (c.2844_2850delAGACAAA in exon 21, p.Lys948Asnfs*9) in a family with eight affected males caused severe mental or developmental retardation and recurrent infections in all; postaxial polydactyly in five, retinitis pigmentosa in three, and a molar tooth sign on brain magnetic resonance imaging (MRI) in two. No heterozygous carrier females had any symptoms similar to those in the affected males. Another mutation (c.2767delG in exon 21, p.Glu923Lysfs*4) was found *de novo* in a 12-year-old male patient with severe mental retardation, macrocephaly, obesity, postaxial polydactyly, and a molar tooth sign on brain MRI (13).

To discuss whether these male patients with hemizygous truncating *OFD1* mutations would have different conditions (OFD1, SGBS2, or JBTS10) or belong to the same syndrome spectrum, we have created a comprehensive list of clinical manifestations in all of them (Table 2) (7, 10, 13). Macrocephaly, polydactyly (postaxial), respiratory insufficiency with recurrent respiratory tract infections in survivors, and severe mental or developmental retardation were shared by all the families (7, 10, 13). Nasal bridge features (depressed or broad) and lip abnormalities (cleft lip, pseudocleft lip, full lips, and prominent philtrum) were shared by the families with OFD1 and JBTS10 (7, 13). Brain malformations including hypoplasia or agenesis of corpus callosum, hypoplasia or agenesis cerebellar vermis as well as posterior fossa abnormalities (large, occipital encephalocele) were also shared by the families with OFD1 and JBTS10 (7, 13). III-5 in the present family was described to have Dandy-Walker malformation on brain ultrasonography. Three patients with JBTS10 were described to have a molar tooth sign on brain MRI, which is the characteristic neuroradiological hallmark of Joubert syndrome (13). Dandy-Walker malformation, typically consisting of agenesis or hypoplasia of cerebellar vermis, a cystic dilatation of the fourth ventricle, and an enlarged posterior fossa with a high position of the tentorium, is usually distinguishable from Joubert syndrome, characterized anatomically by agenesis or hypoplasia of cerebellar vermis and enlargement of the superior cerebellar peduncles and deep interpeduncular fossa resulting from a lack of normal decussation of superior cerebellar peduncular fiber tracts, leading to the characteristic 'molar tooth' appearance on transverse computed tomography and MRI of the midbrain (14); and clinically by hypotonia, developmental retardation, abnormal respiratory patterns, and oculomotor apraxia (15). However, Joubert syndrome could be present in association with Dandy-Walker malformation (15); and in such a case, Dandy-Walker malformation was reported to have initially masked the molar tooth sign because of a cystic dilatation of the fourth ventricle (16). Some authors state that the presence of the molar tooth sign does not, in itself, allow a diagnosis, Joubert syndrome, to be made; but that clinical evidence of the syndrome including hypotonia and developmental retardation accompanied by either abnormal breathing or abnormal eye movements should be present (14, 17). Typical respiratory abnormalities in Joubert syndrome, represented by short alternate episodes of apnea and hyperpnea or episodic hyperpnea alone (18), were not described in the patients with JBTS10, with only one presenting with stridor and intermittent cyanosis soon after birth (13). Abnormal eye movements including oculomotor apraxia were not mentioned in those with JBTS10 (13). In view of these evidences, it is reasonable to consider that the male patients with *OFD1* mutations, identified to date, would belong to a clinical continuum with wide intra- and inter-familial phenotypic variations of a single disorder.

A review by Macca and Franco (4) summarized all reported mutations in OFD1 patients. In total, 99 different mutations (7 genomic deletions and 92 point mutations) were identified, including 67 frameshift mutations (58%), 14 missense mutations (12%), 14 splice-site mutations (12%), 13 nonsense mutations (11%), and an in-frame deletion. Point mutations occur only in the first 17 exons (*OFD1* consists of 23 exons). A significant genotype–phenotype correlation between high-arched/cleft palate and missense and splice-site mutations has been identified (19). In addition, cystic kidney is more frequently associated with mutations in exons 9 and 12 (19). Quantitative PCR analysis of *OFD1* mRNA levels in EBV-LCLs from two families with JBTS10 showed that 30% and 58% of *OFD1* expression remained, suggesting that the mutant mRNA would be subject to nonsense-mediated decay and that the phenotypic variability observed for *OFD1* mutations would be caused by changes in activity of remaining truncated OFD1 protein (13). To date, premature stop codons at 713 in exon 16 (19), 796 in exon 17 (this report), 926 in exon 21 (13), and 956 in exon 21 (13) are associated with survival in males with hemizygous truncating *OFD1* mutations and no or subtle clinical manifestations in females with heterozygous *OFD1* mutations. Heterozygous truncating *OFD1* mutations preserving normal exons 1–16 have been reported in only two families with typical female OFD1 patients: a single-base deletion (c.2349delC in exon 17, p.Ileu784Serfs*85) (20) and a deletion of complete exon 17 (21). Mutations producing longer truncated protein (~ exon 17) might cause a milder form of the disorder that could not be detected in typical female OFD1 patients, but could be detected in male patients with multiple congenital anomalies and probable lethality in childhood.

Table 2. Clinical features of male patients with *OFD1* mutations

	Family 1 (present family)			Family 2[b]	Family 3[c]				Family 4[d] (W07-713)			Family 5[d]	Carrier
Patient	II-4	III-1	III-5	1	IV-1	IV-3	IV-11	6 Patients	III-9	IV-10	6 Patients	(UW87)	19 Females
Age	0d/D	14d/D	1d/D		11 y	18 m/D	3 y/D	D	34 y	3.5 y	D (3)		
Birth weight (g) (gestational age)	2056 (33)	3064 (39)	1704 (32)		3850 (40)	4120 (38)	1915 (35)			3050 (Te)		4090 (41)	
Macrocephaly (>1.5 SD)	+		+		+	+	+	Some				+	
Obesity					+				−	−	−	+	
Craniofacial (87.3%[a])									−	−	−		
Facial anomalies (69.1%[a])													
Prominent forehead	+		+										
Redundant neck skin	+											+	
Hypertelorism	+	+	+	+									
Epicanthus		+											
Short palpebral fissures	+	+											
Nasal bridge features	Dep		Dep						Br	Br		Dep	
Low-set ears	+	+			+				+	+			
Lip abnormalities (32.6%[a])	PCL	CL	PCL	PCL					F_L, PP	F_L, PP		PCL	PCL (1)
Oral													
Palatal abnormalities (49.6%[a])	CSP	CP	CSP	CSP	HP								
Accessory frenulae (63.7%[a])													+ (4)
Tongue abnormalities (84.1%[a])	Nar											MG	Lob (3)
Teeth abnormalities (43.3%[a])													Ir (1)
Skeletal													
Short fingers/brachydactyly					+		+			−		+	
Postaxial polydactyly (3.7%[a])	LtH	BiH		BiHRtBLT		RtH			−	BiHF	BiHF (4)	BiHLtF	
Preaxial polydactyly (19.3%[a])	BiBrHx	BiF		BiBHx	BiBrT								
Respiratory													
Laryngeal anomalies	+												
Respiratory insufficiency	+	+				+				+			
Recurrent infections					+	+	+	+	+	+	+ (6)	+	
Cardiovascular													
Congenital heart defects	ASD, PDA	AVSD	HLHS	AVSD						−			
Genitourinary													
Cystic kidney	−		−		−	−			−	−	−	−	
Urinary tract abnormalities	HU	EUO											
Genital abnormalities	MP, C												
Gastrointestinal													
Esophageal abnormalities			+										
Ophthalmological													
Microphthalmia/microcornea	+												
Persistent papillary membrane		+											

Table 2. Continued

Patient	Family 1 (present family)			Family 2[b]	Family 3[c]				Family 4[d] (W07-713)			Family 5[d] (UW87)	Carrier 19 Females
	II-4	III-1	III-5	1	IV-1	IV-3	IV-11	6 Patients	III-9	IV-10	6 Patients		
Optic disc coloboma		+											
Optic nerve atrophy												+	
Retinal detachment	+												
Retinitis pigmentosa									+	+	+ (1)	−	
Central nervous system (48.4%[a])													
Hydrocephalus		+	+	+	−	−	+						
Gyrus abnormalities	Hp			PM	−	−	−						
Corpus callosum abnormalities		Ag		Ag	−	−	−					Hp	
Cerebellar vermis abnormalities		Ag	Ag		−	−	−		Hp	Hp			
Thick superior cerebellar peduncles					−	−	−		+	+			
Molar tooth sign					−	−	−		+	+		+	
Dandy-Walker malformation			+		−	−	−						
Posterior fossa abnormalities				L	−	−	−			L		EC	
Developmental/mental retardation					S	S	+	S	S	S	+ (All)	S	

+, present; −, absent; blank, data not available; Ag, agenesis; ASD, atrial septal defect; AVSD, atrioventricular septal defect; BHx, bifid halluces; Bi, bilateral; BLT, bifid little toe; Br, broad; C, cryptorchidism; CL, cleft lip; CP, cleft palate; CSP, cleft soft palate; d, days; D, death; Dep, depressed; EC, encephalocele; EUO, ectopic urethral opening; F, foot/feet; FL, full lips; H, hand(s); HF, hands and feet; HLHS, hypoplastic left heart; Hp, hypoplasia; HP, high palate; HU, hydroureter; Hx, halluces; Ir, irregular; L, large; Lob, lobulated; Lt, left; m, months; MG, midline groove; MP, micropenis; Nar, narrowing of the tip of the tongue; PCL, pseudocleft of the upper lip; PDA, patent ductus arteriosus; PM, polymicrogyria; PP, prominent philtrum; Rt, right; S, severe; Te, term; T, thumbs; y, years.

[a]From Macca and Franco (4).

[b]From Goodship et al. (7).

[c]From Budny et al. (10).

[d]From Coene et al. (13).

High-throughput, next-generation sequencing (NGS) has had a tremendous impact on human genetic research (22). Moreover, techniques enabling enrichment of selected regions enable us to use NGS efficiently and to identify the causative genes for a reasonable number of genetic disorders as well as susceptibility genes for complex diseases and health-related traits (23). In particular, X-linked disorders are good candidates for exome sequencing. We recently identified a nonsense mutation in *MCT8* causing X-linked leukoencephalopathy in a family from only two affected male samples (24). We have also identified two possible but inconclusive missense variants (*L1CAM* and *TMEM187*) in a family with an atypical X-linked leukodystrophy from only two affected male samples (25). In this study, exome sequencing accompanied by appropriate bioinformatics techniques and a co-segregation evaluation successfully revealed a disease-causing mutation in *OFD1*, which could not have been assumed to be a candidate based on the clinical manifestations of the affected male patients. Unbiased rapid screening through these technologies is a powerful method for the detection of mutations in unexpected causative genes in undiagnosed patients with multiple congenital malformations.

In conclusion, we have identified a causative splicing mutation in *OFD1*, through exome sequencing, in a family with three males having an 'unclassified' X-linked lethal congenital malformation syndrome. The affected males manifested severe multisystem complications in addition to the cardinal features of OFD1 and the carrier female showed only subtle features of OFD1. The present patients, as well as the previously reported male patients from four families (one with clinical OFD1; one with SGBS2 and an *OFD1* mutation; two with JBTS10 and *OFD1* mutations), would belong to a single syndrome spectrum caused by truncating *OFD1* mutations, presenting with craniofacial features (macrocephaly, depressed or broad nasal bridge, and lip abnormalities), postaxial polydactyly, respiratory insufficiency with recurrent respiratory tract infections in survivors, severe mental or developmental retardation, and brain malformations (hypoplasia or agenesis of corpus callosum and/or cerebellar vermis and posterior fossa abnormalities).

Acknowledgements

The authors are grateful to the family for their participation in this study. The authors are also thankful to Prof Germana Meroni (Cluster in Biomedicine, Trieste) for mutation analysis of *MID1*, Dr Takeshi Futatani (Department of Pediatrics, Toyama Prefectural Central Hospital, Toyama, Japan), Dr Masahiko Kawabata (Department of Internal Medicine, Toyama Prefectural Central Hospital, Toyama, Japan), and Dr Akio Uchiyama (Department of Pathology, Toyama Prefectural Central Hospital, Toyama, Japan) for collecting clinical information; Dr Gen Nishimura (Department of Radiology, Tokyo Metropolitan Children's Medical Center) for helping radiological assessment; and Miss Junko Kunimi (Department of Medical Genetics, Shinshu University School of Medicine, Matsumoto, Japan) and Dr Shin-ya Nishio (Department of Otolaryngology, Shinshu University School of Medicine, Matsumoto, Japan) for their technical assistance. This work was supported by research grants from the Ministry of Health, Labour and Welfare (T. K., Y. F., H. S., N. Mi., and N. Ma.), the Japan Science and Technology Agency (N. Ma.), the Strategic Research Program for Brain Sciences (N. Ma.) and a Grant-in-Aid for Scientific Research on Innovative Areas (Foundation of Synapse and Neurocircuit Pathology) from the Ministry of Education, Culture, Sports, Science and Technology of Japan (N. Ma.), a Grant-in-Aid for Scientific Research from Japan Society for the Promotion of Science (N. Ma.), a Grant-in-Aid for Young Scientist from Japan Society for the Promotion of Science (H. S. and N. Mi.) and a grant from the Takeda Science Foundation (N. Mi. and N. Ma.). This work was performed at the Advanced Medical Research Center, Yokohama City University, Japan.

Y. T., H. D., H. S., and N. Mi. performed the genetic analysis; T. K., K. H., Y. N., K. W., and Y. F. evaluated clinical aspects of the family, recruited samples, and prepared them for the analysis. Y. T., T. K. and N. Ma. wrote the manuscript.

Ethics approval

The work was approved by the Yokohama City University (Faculty of Medicine) and the Shinshu University (School of Medicine). Patient consent was obtained.

References

1. Papillon-Leage M, Psaume J. Une malformation hereditaire de la muquese buccale: brides et freins anomaux. Rev Stomatol 1954: 55: 209–227.
2. Gorlin RJ, Psaume J. Orofaciodigital dysostosis: a new syndrome. A study of 22 cases. J Pediatr 1962: 61: 520–530.
3. Ferrante MI, Giorgio G, Feather SA et al. Identification of the gene for oral-facial-digital type I syndrome. Am J Hum Genet 2001: 68: 569–576.
4. Macca M, Franco B. The molecular basis of oral-facial-digital syndrome, type 1. Am J Med Genet C 2009: 151C: 318–325.
5. Toriello HV, Franco B. Oral-facial-digital syndrome type I. In: Pagon RA, Bind TD, Dolan CR, Stephans K, Adam MP, eds. GeneReviews at genetests: Medical Genetics Information Resource (database online). Seattle, WA: Copyright, University of Washington, 1993–2011, from http://www.genetests.org. Accessed on July 23, 2011.
6. Morleo M, Franco B. Dosage compensation of the mammalian X-chromosome influences the phenotypic variability of X-linked dominant male-lethal disorders. J Med Genet 2008: 45: 401–408.
7. Goodship J, Platt J, Smith R, Burn J. A male with type I orofaciodigital syndrome. J Med Genet 1991: 28: 691–694.
8. Fontanella B, Russolillo G, Meroni G. MID1 mutations in patients with X-linked Opitz G/BBB syndrome. Hum Mutat 2008: 29: 584–594.
9. Nishimura-Tadaki A, Wada T, Bano G et al. Breakpoint determination of X;autosome balanced translocations in four patients with premature ovarian failure. J Hum Genet 2011: 56: 156–160.
10. Budny B, Chen W, Omran H et al. A novel X-linked recessive mental retardation syndrome comprising macrocephaly and ciliary dysfunction is allelic to oral-facial-digital type I syndrome. Hum Genet 2006: 120: 171–178.
11. Terespolsky D, Farrell SA, Siegel-Bartelt J, Weksberg R. Infantile lethal variant of Simpson-Golabi-Behmel syndrome associated with hydrops fetalis. Am J Med Genet 1995: 59: 329–333.
12. Brzustowicz LM, Farrell S, Khan MB, Weksberg R. Mapping of a new SGBS locus to chromosome Xp22 in a family with a severe form of Simpson-Golabi-Behmel syndrome. Am J Hum Genet 1999: 65: 779–783.
13. Coene KL, Roepman R, Doherty D et al. OFD1 is mutated in X-linked Joubert syndrome and interacts with LCA5-encoded lebercilin. Am J Hum Genet 2009: 85: 465–481.
14. McGraw P. The molar tooth sign. Radiology 2002: 229: 671–672.
15. Chance PF, Cavalier L, Satran D, Pellegrino JE, Koenig M, Dobyns WB. Clinical nosologic and genetic aspects of Joubert and related syndromes. J Child Neurol 1999: 14: 660–666.

16. Sartori S, Ludwig K, Fortuna M et al. Dandy-Walker malformation masking the molar tooth sign: an illustrative case with magnetic resonance imaging follow-up. J Child Neurol 2010: 25: 1419–1422.
17. Barkovich AJ. Anomalies with cerebellar dysgenesis: vermian dysgenesis. In: Barkovich AJ, ed. Pediatric neuroimaging, 4th edn. Lippincott Williams & Wilkins, Philadelphia 2005: 391–396.
18. Brancati F, Dallapiccola B, Valente EM. Joubert syndrome and related disorders. Orphanet J Rare Dis 2010: 5: 20.
19. Prattichizzo C, Macca M, Novelli V et al. Mutational spectrum of the oral-facial-digital type I syndrome: a study on a large collection of patients. Hum Mutat 2008: 29: 1237–1246.
20. Thauvin-Robinet C, Cossée M, Cormier-Daire V et al. Clinical, molecular, and genotype-penotype correlation studies from 25 cases of oral-facial-digital syndrome type 1: a French and Belgian collaborative study. J Med Genet 2006: 43: 54–61.
21. Thauvin-Robinet C, Franco B, Saugier-Veber P et al. Genomic deletions of *OFD1* account for 23% of oral-facial-digital type 1 syndrome after negative DNA sequencing. Hum Mutat 2008: 30: E320–E329.
22. Shendure J, Ji H. Next-generation DNA sequencing. Nat Biotechnol 2008: 26: 1135–1145.
23. Bamshad MJ, Ng SB, Bigham AW et al. Exome sequencing as a tool for Mendelian disease gene discovery. Nat Rev Genet 2011: 12: 745–755.
24. Tsurusaki Y, Osaka H, Hamanoue H et al. Rapid detection of a mutation causing X-linked leukodystrophy by exome sequencing. J Med Genet 2011: 48: 606–609.
25. Tsurusaki Y, Okamoto N, Suzuki Y et al. Exome sequencing of two patients in a family with atypical X-linked leukodystrophy. Clin Genet 2011: 80: 161–166.

Journal of Human Genetics (2012) 57, 207–211

www.nature.com/jhg

ORIGINAL ARTICLE

Missense mutations in the DNA-binding/dimerization domain of *NFIX* cause Sotos-like features

Yuriko Yoneda[1], Hirotomo Saitsu[1], Mayumi Touyama[2], Yoshio Makita[3], Akie Miyamoto[4], Keisuke Hamada[5], Naohiro Kurotaki[6], Hiroaki Tomita[7], Kiyomi Nishiyama[1], Yoshinori Tsurusaki[1], Hiroshi Doi[1], Noriko Miyake[1], Kazuhiro Ogata[5], Kenji Naritomi[8] and Naomichi Matsumoto[1]

Sotos syndrome is characterized by prenatal and postnatal overgrowth, characteristic craniofacial features and mental retardation. Haploinsufficiency of *NSD1* causes Sotos syndrome. Recently, two microdeletions encompassing *Nuclear Factor I-X (NFIX)* and a nonsense mutation in *NFIX* have been found in three individuals with Sotos-like overgrowth features, suggesting possible involvements of *NFIX* abnormalities in Sotos-like features. Interestingly, seven frameshift and two splice site mutations in *NFIX* have also been found in nine individuals with Marshall–Smith syndrome. In this study, 48 individuals who were suspected as Sotos syndrome but showing no *NSD1* abnormalities were examined for *NFIX* mutations by high-resolution melt analysis. We identified two heterozygous missense mutations in the DNA-binding/dimerization domain of the NFIX protein. Both mutations occurred at evolutionally conserved amino acids. The c.179T>C (p.Leu60Pro) mutation occurred *de novo* and the c.362G>C (p.Arg121Pro) mutation was inherited from possibly affected mother. Both mutations were absent in 250 healthy Japanese controls. Our study revealed that missense mutations in *NFIX* were able to cause Sotos-like features. Mutations in DNA-binding/dimerization domain of NFIX protein also suggest that the transcriptional regulation is abnormally fluctuated because of *NFIX* abnormalities. In individuals with Sotos-like features unrelated to *NSD1* changes, genetic testing of *NFIX* should be considered.
Journal of Human Genetics (2012) **57**, 207–211; doi:10.1038/jhg.2012.7; published online 2 February 2012

Keywords: DNA-binding/dimerization domain; missense mutation; *NFIX*; Sotos syndrome

INTRODUCTION

Sotos syndrome (MIM #117550) is an overgrowth syndrome characterized by tall stature and/or macrocephaly, distinctive facial appearance and mental retardation.[1] A *de novo* t(5;8)(q35;q24.1) translocation in a patient with Sotos syndrome revealed disruption of *NSD1* at 5q35. Subsequent identification of nonsense, frameshift and submicroscopic deletion mutations of *NSD1* in patients with Sotos syndrome clearly showed that haploinsufficiency of *NSD1* causes Sotos syndrome.[2] *NSD1* encodes nuclear receptor-binding SET domain protein 1, which functions as a histone methyltransferase that activates and represses transcription through chromatin modification.[3] The diagnosis of Sotos syndrome is established by confirming *NSD1* abnormalities,[4] and abnormalities of *NSD1* causes up to 90% of Sotos syndrome cases. However, a part of patients with suspected Sotos syndrome are known to show no abnormalities in *NSD1*,[5] suggesting involvement of another gene.

Recently it was reported that two patients with Sotos-like overgrowth features possessed microdeletions encompassing *Nuclear Factor I-X (NFIX)* at 19p13.2. In addition, a nonsense mutation in *NFIX* was identified in one patient with Sotos-like features.[6] Interestingly, frameshift and donor-splice site mutations were also identified in Marshall–Smith syndrome (MIM 602535) that is osteochondysplasia syndrome characterized by accelerated skeletal maturation, relative failure to thrive, respiratory difficulties, mental retardation and unusual facial features.[7] Therefore, *NFIX* mutations could cause either Sotos-like features or Marshall–Smith syndrome. Whereas the transcripts possessing the nonsense mutation in a patient with Sotos-like features suffered from the nonsense-mediated mRNA decay, transcripts of mutated alleles (by a donor-spice site and two frameshift mutations) in patients with Marshall–Smith syndrome escaped from the nonsense-mediated mRNA decay surveillance and could be translated, suggesting that haploinsufficiency of *NFIX* leads to

[1]Department of Human Genetics, Yokohama City University Graduate School of Medicine, Yokohama, Japan; [2]Department of Pediatrics, Okinawa Child Development Center, Okinawa, Japan; [3]Education Center, Asahikawa Medical University, Asahikawa, Japan; [4]Department of Pediatrics, Hokkaido Asahikawa Habilitation Center for Disabled Children, Asahikawa, Japan; [5]Department of Biochemistry, Yokohama City University Graduate School of Medicine, Yokohama, Japan; [6]Department of Neuropsychiatry, Nagasaki University Graduate School of Biomedical Sciences, Nagasaki, Japan; [7]Department of Biological Psychiatry, Tohoku University Graduate School of Medicine, Sendai, Japan and [8]Department of Medical Genetics, University of the Ryukyus Faculty of Medicine, Nishihara, Japan
Correspondence: Dr N Matsumoto, Department of Human Genetics, Yokohama City University Graduate School of Medicine, Fukuura 3-9, Kanazawa-ku, Yokohama 236-0004, Japan.
E-mail: naomat@yokohama-cu.ac.jp
Received 9 September 2011; revised 21 November 2011; accepted 5 January 2012; published online 2 February 2012

Sotos-like features and dominant-negative effects of the truncated NFIX proteins cause Marshall–Smith syndrome.[6]

In this study, we screened for *NFIX* mutations in 48 Japanese patients who were suspected as Sotos syndrome, but showed neither deletions nor mutations in *NSD1*. Detailed genetic and clinical data are presented.

MATERIALS AND METHODS

Subjects

A total of 48 patients suspected as Sotos syndrome were analyzed for *NFIX* mutations. *NSD1* investigation by sequencing and fluorescent *in situ* hybridization analysis was negative in these patients. In this study, the patients presenting with cardinal features of Sotos syndrome (specific craniofacial features, intellectual disability and overgrowth to same extent) but showing no *NSD1* abnormalities are referred as those with 'Sotos-like features'. Experimental protocols were approved by the Committee for Ethical issues at Yokohama City University School of Medicine. All individuals were investigated in agreement with the requirements of Japanese regulations.

Mutation analysis

Genomic DNA was isolated from peripheral blood leukocytes according to standard methods. DNA for mutation screening was amplified by illustra GenomiPhi V2 DNA Amplification Kit (GE Healthcare, Buckinghamshire, UK). Sequencing of exon 1 and high-resolution melting curve (HRM) analysis of exon 2–9 covering the *NFIX* coding region (GenBank accession number NM_002501.2) were performed. For exon 1, the 12 μl PCR mixture contained 30 ng DNA, 0.3 μM each primer, 0.4 mM each dNTP, 1× PCR buffer for KOD FX and 0.3 U KOD FX polymerase (Toyobo, Osaka, Japan). For exons 2–9, real-time PCR and HRM analysis were serially performed in 12 μl mixture on Rotor-Gene Q (QIAGEN, Hilden, Germany). For exon 7, the PCR mixture contained 30 ng DNA, 0.3 μM each primer, 0.4 mM each dNTP, 0.36 μl SYTO9 (Invitrogen, Carlsbad, CA, USA), 0.4 mM each dNTP, 1× PCR buffer for KOD FX and 0.3 U KOD FX polymerase (Toyobo). For the remaining exons, the PCR mixture contained 30 ng DNA, 0.25 μM each primer, 0.36 μl SYTO9 (Invitrogen), 0.2 mM each dNTP, 1× ExTaq buffer and 0.375 U ExTaq HS (Takara, Otsu, Japan). Primers and conditions of PCR are shown in Supplementary Table 1. The PCR products showing an aberrant melting curve were sequenced. All the novel mutations in DNA amplified by GenomiPhi were verified by sequencing of PCR products using genomic DNA as a template. Mutations were checked in 250 Japanese normal controls (500 alleles) by HRM analysis.

Parentage testing

For the family showing *de novo* mutations, parentage was confirmed by microsatellite analysis as previously described.[8] Biological parentage was judged if more than four informative markers were compatible and other uninformative markers showed no discrepancies.

Prediction of functional effect

The effect of the mutations for protein features was predicted by following web-based prediction tools: SIFT (http://sift.jcvi.org/), PolyPhen (http://genetics.bwh.harvard.edu/pph/), PolyPhen-2 (http://genetics.bwh.harvard.edu/pph2/), Mutation Taster (http://www.mutationtaster.org/) and Align GVGD (http://agvgd.iarc.fr/agvgd_input.php).

RESULTS

NFIX mutations

Two heterozygous missense mutations were identified. The c.179T>C (p.Leu60Pro) mutation in patient 1 were not found in her parents, indicating that the mutation occurred *de novo* (Figure 1a). Biological parentage was confirmed by several microsatellite markers (data not shown). The c.362G>C (p.Arg121Pro) mutation in patient 2 was found in his mother (Figure 1a). These two mutations occurred at evolutionary conserved amino acids (Figure 1b) and were absent in 250 Japanese normal controls. Interestingly, the missense changes were located in DNA-binding/dimerization domain of the NFIX protein (Figure 1c). Evaluation with web-based prediction tools strongly suggested that these substitutions are pathogenic (Supplementary Table 2).

Clinical information of the patients

Patient 1 is a product of unrelated healthy parents. The body weight at birth was 2816 g (−0.6 s.d.), height 48.8 cm (0 s.d.) and OFC 33.5 cm (+0.3 s.d.). Neonatal hypotonia was recognized. At 17 months of age, her weight was 9.24 kg (−0.5 s.d.), height 84.9 cm (+2 s.d.) and OFC 48 cm (+1.2 s.d.). The facial appearance showed long/narrow and triangular face, high forehead, midface hypoplasia, prominent ears, epicanthal folds, strabismus, down-slanting palpebral fissures, short nose with anteverted nares, prominent long philtrum, everted lower lip and narrow palate (Figure 1d). Large hands/feet, prominent fingertips, pectus excavatum were also noted. Her primary dentition started at 7 months of age and was completed by 17 months of age. Bone age was estimated as 3 years at 17 months of age and as 5 years at 3 years of age. Bullet-shaped phalanges, which are typical features of Marshall–Smith syndrome, were not observed. She was initially diagnosed as Sotos syndrome. She showed mental retardation and severe developmental delay with developmental quotients of 19. Scoliosis was noted at 18 months of age and surgically treated for several times. Complex partial seizures were noted at 4 years of age and were controlled with phenytoin and zonisamide. At present (17 years of age), prognathia was observed (Figure 1e). Her weight was 40 kg (−2 s.d.) and height 156.5 cm (−0.2 s.d.).

Patient 2 is a male at age of 20 years. The birth weight was 2938 g (−0.4 s.d.), height 51 cm (+0.8 s.d.) and OFC 35.5 cm (+1.4 s.d.). Respiratory insufficiency was noted, but no visceral malformations were pointed out. Bilateral tubing therapy was performed for recurrent bilateral exudative otitis media at 4 years of age. At 14 years of age, his weight was 58.1 kg (+0.6 s.d.) and height 185.7 cm (+3.5 s.d.). Mental retardation was evident as the IQ score (Tanaka–Binet intelligence test) was 59. Craniofacial features included high forehead, down-slanting palpebral fissures and prognathia. He was suspected as Sotos syndrome. His mother showed tall stature, suggesting that c.362G>C led to overgrowth in the mother. Unfortunately, further details of clinical features in the mother are unavailable. Clinical information of two patients is summarized in Table 1.

DISCUSSION

NFIX is a member of the nuclear factor I (NFI) family proteins, which are implicated as site-specific DNA-binding proteins known to function in viral DNA replication and gene expression regulation.[9] NFI proteins form homo- or heterodimers and bind to the palindromic DNA consensus sequence through its N-terminal DNA-binding/dimerization domain.[10] Point mutations in DNA-binding/dimerization domain of NFI protein have been shown to cause loss of dimerization, DNA-binding and replication activities,[11] highlighting the importance of structural integrity of DNA-binding/dimerization domain. It has been reported that the DNA binding domain of SMADs and NFI transcription factors shared considerable structural similarity, and the secondary structure of the DNA-binding domain of NFI was estimated based on that of SMADs.[12] In this study, we identified two heterozygous missense mutations, the c.179T>C (p.Leu60Pro) and the c.362G>C (p.Arg121Pro), in the DNA-binding/dimerization domain. Of note, two mutations are estimated to be localized within α-helical region of DNA-binding domain and at evolutionally conserved amino acids between SMADs and NFI.[12] In addition, two mutations cause substitutions to a proline residue,

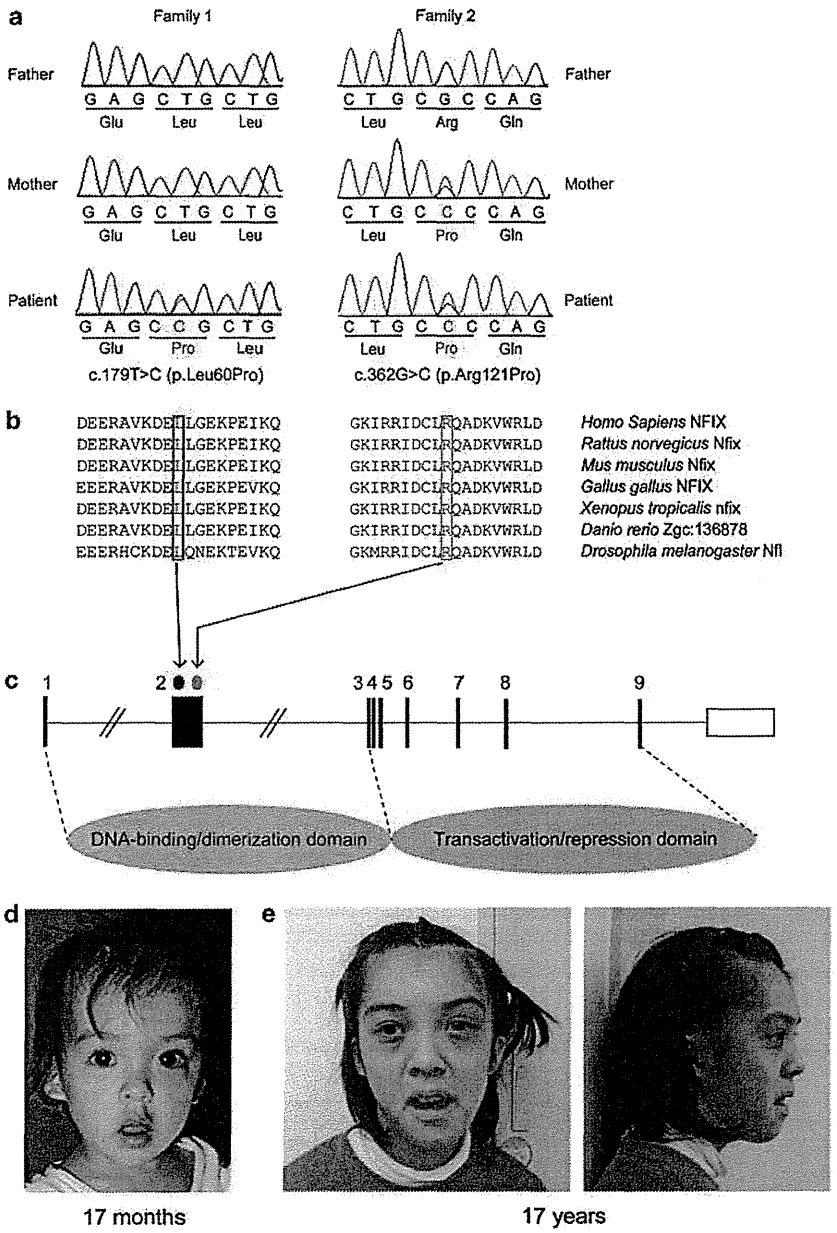

Figure 1 Missense mutations in *NFIX* in individuals with Sotos-like features. (**a**) Electropherogram of family 1 (left) and family 2 (right). The c.179T>C (p.Leu60Pro) mutation occured *de novo*. The c.362G>C (p.Arg121Pro) mutation was inherited from his mother. (**b**) An amino-acid sequence alignments of NFIX protein including amino-acid positions 60 and 121. Protein sequences were obtained through the NCBI protein database and multiple sequence alignment was performed by CLUSTALW web site (http://clustalw.ddbj.nig.ac.jp/). (**c**) Schematic representation of *NFIX* consisting of nine exons. UTR and coding exons are indicated by open and filled rectangles, respectively. The location of mutations is indicated by red (c.179T>C) and blue (c.362G>C) dots. At the bottom, C-terminal DNA-binding/dimerization domain and N-terminal transactivation/repression domain are depicted. Both the c.179T>C and c.362G>C mutations are located in exon 2 encoding a part of DNA-binding/dimerization domain. (**d**) Facial appearance of patient 1 at 17 months of age, showing long/narrow and triangular face, down slanting, short nose with anteverted nares and everted lower lip. (**e**) At 17 years of age, prognathia was noted in patient 1.

which is a unique amino acid characterized by imino radical. Proline has a pyrrolidine ring that restricts the available conformational space; therefore, it has effects on chain conformation and the process of protein folding.[13] Thus, it is very likely that two mutations could affect DNA-binding activity of NFIX protein through conformational changes of the DNA-binding domain.

Because *NFIX* mutations could cause both Marshall–Smith syndrome and Sotos-like features,[6] it is great concern to which of them two patients with missense mutations could be classified. Main clinical features of Sotos syndrome are childhood overgrowth including tall stature and/or macrocephaly, characteristic face and mental retardation. Other minor features are scoliosis, hypotonia in infancy, seizures,

Table 1 Clinical features of two patients with missense mutations in *NFIX*

				Reported by Malan et al.[6]		
		Patient 1	*Patient 2*	*Patient A*	*Patient B*	*Patient C*
Genetics	*NFIX deletion/mutation*	*c.179T>C*	*c.362G>C*	*del 19p13.3*	*del 19p13.3*	*c.568C>T*
Epidemiology	Age at last evaluation (years)	17	14	14	10	27
	Sex	F	M	M	M	F
	Mat/pat age	48/52	?/?	31/33	25/30	31/31
Prenatal growth	Birth weight (g)	2816 (−0.6 s.d.)	2938 (−0.4 s.d.)	4500 (>95)	3110 (10–50)	3600 (50–90)
	Birth height (cm)	48.8 (0 s.d.)	51 (+0.8 s.d.)	53 (95)	49 (50)	52 (95)
	OFC (cm)	33.5 (+0.3 s.d.)	35.5 (+1.4 s.d.)	38 (>95)	33.5 (10)	37.5 (>95)
Postnatal growth	Weight (kg)	9.24 (−0.5 s.d.)[a]	58.1 (+0.6 s.d.)[b]	>P98	>P98	>P98
	Height (cm)	84.9 (+2 s.d.)[a]	185.7 (+3.5 s.d.)[b]	>P98	>P98	>P98
Development						
SS	Autistic traits	−	−	+	+	+
	Behavioral anomalies	NA	−	+	+	+
	Motor retardation	+	+	+	−	−
	Hypotonia	+	+	+	+	−
Overlapped	Mental retardation	+	+	+	+	+
	Degree of delay	DQ19	IQ42	NA	NA	NA
	Speech delay	+	+	+	+	+
	First words (months)	24	18	NA	NA	NA
Craniofacial features						
SS	Long/narrow face	+	−	+	+	+
	Down-slanting palpebral fissures	+	+	+	−	+
	Small mouth	NA	−	+	−	+
	Prognathia	+	+	+	−	−
Overlapped	High forehead	+	+	+	+	+
MSS	Everted lower lip	+	−	+	−	+
	Underdeveloped midface	+	−	NA	NA	NA
	Proptosis	NA	−	NA	NA	NA
	Short nose	+	−	NA	NA	NA
	Prominent premaxilla	NA	−	NA	NA	NA
	Gum hypertrophy	+[c]	−	NA	NA	NA
	Retrognathia	−	−	NA	NA	NA
Eyes						
SS	Hypermotropia	−	−	+	+	−
	Strabismus	+	−	+	−	+
	Nystagmus	−	−	−	−	+
	Astigmatism	NA	NA	−	+	−
MSS	Myopia	NA	−	NA	NA	NA
	Blue sclerae	NA	−	NA	NA	NA
Musculo-skeletal abnormalities						
SS	Abdominal wall hypotonia	−	−	+	−	+
	Pectus excavatum	+	−	+	+	−
	Coxa valga	−	−	+	+	−
Overlapped	Scoliosis	+	−	+	−	+
	Advanced bone age	+	NA	+	+	+
MSS	Abnormal bone maturation	NA	NA	NA	NA	NA
	Bone fractures	−	−	NA	NA	NA
	Kyphosis	−	−	NA	NA	NA
	Umbilical hernia	−	−	NA	NA	NA

Abbreviations: F, female; M, male; Mat/pat, maternal/paternal; MSS, Marshall–Smith syndrome; NA, not ascertained; OFC, Occipitofrontal circumference; SS, Sotot's syndrome.
Growth of patients 1 and 2 is indicated with s.d. and that of patients in the report of Malan *et al.*[6] is indicated with percentile.
[a]At 17 months.
[b]At 14 years.
[c]Suggested the possibility of the adverse drug reaction.

cardiac defect and genitourinary anomalies.[5] On the other hand, main clinical features of Marshall–Smith syndrome are moderate to severe developmental delay with absent or limited speech, unusual behavior, disharmonic bone maturation, respiratory compromise secondary to upper airway obstruction, short stature and kyphoscoliosis.[14] One of remarkable differences between Sotos syndrome and Marshall–Smith syndrome is facial appearances. Although both syndromes has high forehead, Sotos syndrome has a long/narrow face, triangular shaped face with a prominent chin, down-slanting of the palpebral fissures,[1,4–5] whereas Marshall–Smith syndrome has proptosis, underdeveloped midface and prominent premaxilla.[7,14] In patient 1, although some characteristic features of Marshall–Smith syndrome such as everted lower lip, short nose and midface hypoplasia were observed, overall facial appearance, overgrowth features at 17 month of age, scoliosis, hypotonia and seizures were consistent with Sotos syndrome. Similarly, in patient 2, the facial appearance, tall stature and macrocephaly were consistent with Sotos syndrome. In both patients, their body weights were relatively low in comparison with their heights. This is consistent with the fact that, throughout childhood and early adolescence, the height was usually more significantly increased than weight in Sotos patients.[15] In addition, our patients did not show respiratory difficulties, one of specific features in Marshall–Smith syndrome, which cause early death in the neonatal period or early infancy.[7] Thus missense mutations in the DNA-binding/dimerization domain, which may lead to loss of transcriptional regulation by NFIX protein, could cause Sotos-like syndrome in two patients.

Many clinical features including tall statue, mental retardation, speech delay and high forehead are shared between our patients and three patients reported by Malan *et al.*[6] with *NFIX* abnormalities. The recognizable difference is autistic traits. Autistic traits are not observed in our patients but all of Malan *et al.*'s[6] patients. Thus there is a possibility that autistic traits are caused by haploinsufficiency of *NFIX* in Malan *et al.*'s[6] patients, but not by misssense mutations in the DNA-binding/dimerization domain. However, identification of a greater number of cases with *NFIX* mutations is required to confirm this hypothesis.

In conclusion, our report provides further evidences that *NFIX* is a causative gene for Sotos-like features. Abnormalities of *NSD1* are found in majority of Sotos syndrome cases and aberration of other genes including *NFIX* may be found in the minority of Sotos syndrome/Sotos-like features. Genetic testing of *NFIX* should be considered in such patients if no *NSD1* abnormalities were identified.

CONFLICT OF INTEREST

The authors declare no conflict of interest.

ACKNOWLEDGEMENTS

We thank the patients and their family members for their participation in this study. This work was supported by Research Grants from the Ministry of Health, Labour and Welfare (HS, N Miyake and N Matsumoto) and the Japan Science and Technology Agency (N Matsumoto), a Grant-in-Aid for Young Scientist from the Japan Society for the Promotion of Science (HS, HD and N Miyake) and a Grant-in-Aid for Scientific Research from Japan Society for the Promotion of Science (N Matsumoto).

1 Leventopoulos, G., Kitsiou-Tzeli, S., Kritikos, K., Psoni, S., Mavrou, A., Kanavakis, E. *et al.* A clinical study of Sotos syndrome patients with review of the literature. *Pediatr. Neurol.* **40,** 357–364 (2009).
2 Kurotaki, N., Imaizumi, K., Harada, N., Masuno, M., Kondoh, T., Nagai, T. *et al.* Haploinsufficiency of *NSD1* causes Sotos syndrome. *Nat. Genet.* **30,** 365–366 (2002).
3 Rayasam, G. V., Wendling, O., Angrand, P. O., Mark, M., Niederreither, K., Song, L. *et al. NSD1* is essential for early post-implantation development and has a catalytically active SET domain. *EMBO J.* **22,** 3153–3163 (2003).
4 Visser, R. & Matsumoto, N. in *Inborn Errors of Development* (eds Epstein, C. J., Erickson, R. P., Wynshaw-Boris, A.) 1032–1037 (Oxford University Press, New York, 2008).
5 Tatton-Brown, K. & Rahman, N. Sotos syndrome. *Eur. J. Hum. Genet.* **15,** 264–271 (2007).
6 Malan, V., Rajan, D., Thomas, S., Shaw, A. C., Louis Dit Picard, H., Layet, V. *et al.* Distinct effects of allelic *NFIX* mutations on nonsense-mediated mRNA decay engender either a Sotos-like or a Marshall-Smith syndrome. *Am. J. Hum. Genet.* **87,** 189–198 (2010).
7 Adam, M. P., Hennekam, R. C., Keppen, L. D., Bull, M. J., Clericuzio, C. L., Burke, L. W. *et al.* Marshall-Smith syndrome: natural history and evidence of an osteochondrodysplasia with connective tissue abnormalities. *Am. J. Med. Genet. A.* **137,** 117–124 (2005).
8 Saitsu, H., Kato, M., Mizuguchi, T., Hamada, K., Osaka, H., Tohyama, J. *et al. De novo* mutations in the gene encoding STXBP1 (MUNC18-1) cause early infantile epileptic encephalopathy. *Nat. Genet.* **40,** 782–788 (2008).
9 Gronostajski, R. M. Roles of the NFI/CTF gene family in transcription and development. *Gene* **249,** 31–45 (2000).
10 Kruse, U. & Sippel, A. E. Transcription factor nuclear factor I proteins form stable homo- and heterodimers. *FEBS Lett.* **348,** 46–50 (1994).
11 Armentero, M. T., Horwitz, M. & Mermod, N. Targeting of DNA polymerase to the adenovirus origin of DNA replication by interaction with nuclear factor I. *Proc. Natl. Acad. Sci. USA* **91,** 11537–11541 (1994).
12 Stefancsik, R. & Sarkar, S. Relationship between the DNA binding domains of SMAD and NFI/CTF transcription factors defines a new superfamily of genes. *DNA Seq.* **14,** 233–239 (2003).
13 MacArthur, M. W. & Thornton, J. M. Influence of proline residues on protein conformation. *J. Mol. Biol.* **218,** 397–412 (1991).
14 Shaw, A. C., van Balkom, I. D., Bauer, M., Cole, T. R., Delrue, M. A., Van Haeringen, A. *et al.* Phenotype and natural history in Marshall-Smith syndrome. *Am. J. Med. Genet. A* **152A,** 2714–2726 (2010).
15 Cole, T. R. & Hughes, H. E. Sotos syndrome: a study of the diagnostic criteria and natural history. *J. Med. Genet.* **31,** 20–32 (1994).

Supplementary Information accompanies the paper on Journal of Human Genetics website (http://www.nature.com/jhg)

Journal of Human Genetics (2012) 57, 197–201

www.nature.com/jhg

ORIGINAL ARTICLE

A family of oculofaciocardiodental syndrome (OFCD) with a novel *BCOR* mutation and genomic rearrangements involving *NHS*

Yukiko Kondo[1], Hirotomo Saitsu[1], Toshinobu Miyamoto[2], Kiyomi Nishiyama[1], Yoshinori Tsurusaki[1], Hiroshi Doi[1], Noriko Miyake[1], Na-Kyung Ryoo[3], Jeong Hun Kim[3], Young Suk Yu[3] and Naomichi Matsumoto[1]

Oculofaciocardiodental syndrome (OFCD) is an X-linked dominant disorder associated with male lethality, presenting with congenital cataract, dysmorphic face, dental abnormalities and septal heart defects. Mutations in *BCOR* (encoding BCL-6-interacting corepressor) cause OFCD. Here, we report on a Korean family with common features of OFCD including bilateral 2nd–3rd toe syndactyly and septal heart defects in three affected females (mother and two daughters). Through the mutation screening and copy number analysis using genomic microarray, we identified a novel heterozygous mutation, c.888delG, in the *BCOR* gene and two interstitial microduplications at Xp22.2–22.13 and Xp21.3 in all the three affected females. The *BCOR* mutation may lead to a premature stop codon (p.N297IfsX80). The duplication at Xp22.2–22.13 involved the *NHS* gene causative for Nance–Horan syndrome, which is an X-linked disorder showing similar clinical features with OFCD in affected males, and in carrier females with milder presentation. Considering the presence of bilateral 2nd–3rd toe syndactyly and septal heart defects, which is unique to OFCD, the mutation in *BCOR* is likely to be the major determinant for the phenotypes in this family.
Journal of Human Genetics (2012) **57,** 197–201; doi:10.1038/jhg.2012.4; published online 2 February 2012

Keywords: *BCOR*; congenital cataract; frameshift mutation; genomic rearrangement; Nance-Horan syndrome; *NHS*; oculofaciocardiodental syndrome

INTRODUCTION

Oculofaciocardiodental syndrome (OFCD, Mendelian Inheritance in Man (MIM) #300166), an X-linked dominant disorder, is characterized by ocular, facial, cardiac and dental abnormalities associated with male lethality.[1,2] Mutations in the BCL-6 corepressor gene (*BCOR*, MIM *300485) at Xp11.4 cause OFCD.[3] *BCOR/Bcor* is ubiquitously expressed in human tissues and is strongly and specifically expressed in the eye, brain, neural tube and branchial arches during mouse embryonic development, which are affected in OFCD.[4,5] In 2009, Hilton *et al.*[6] clinically reviewed 35 cases with *BCOR* mutations and summarized the frequency of phenotypes: congenital cataract (100%), microphthalmia and/or microcornea (82%), facial dysmorphism (96%) including long narrow face and high nasal bridge, cardiac anomalies (74%, commonly septal defects), dental abnormalities (100%) such as delayed and/or primary dentition, root radiculomegaly, and absent/duplicated/fused teeth and mental retardation (18%).[6] Additionally, skeletal abnormalities such as 2nd–3rd toe syndactyly, hammer toes, and radioulnar synostosis are also observed in 97% patients. Various types of mutations in *BCOR* have been described including nonsense, small insertions or deletions and splice site mutations, suggesting that the loss of functions (null allele) might result in OFCD. In addition, microdeletions involving *BCOR* have been also reported in individuals with OFCD. Most mutations predicted to generate premature stop codons, likely suffering from nonsense-mediated mRNA decay, although nonsense-mediated mRNA decay was unable to be confirmed because of the severe skewed X-inactivation in blood leukocytes.[3,6]

Nance–Horan syndrome (NHS) is an X-linked cataract-dental syndrome (MIM #302350) characterized by congenital cataract, dental abnormalities, facial dysmorphism and mental retardation.[7] Congenital cataract in affected male usually requires early surgery.[8] Dental abnormalities include maxillary and mandibular diastema of both central and lateral incisors, and screwdriver-shaped teeth because of narrow gingival and incisal margins.[9] Carrier females typically display posterior Y-sutural lens opacities, and the dental and facial anomalies of the syndrome may be observed, but with a milder presentation.[8] Mutations in *NHS* (MIM *300457) at Xp21.1-p22.3 cause NHS.[9–11] The most pathogenic mutations are truncating mutations. Coccia *et al.*[8] reported complex duplication-triplication rearrangements of the *NHS* gene in a family with congenital cataract and congenital

[1]Department of Human Genetics, Yokohama City University Graduate School of Medicine, Yokohama, Japan; [2]Department of Obstetrics and Gynecology, Asahikawa Medical College, Asahikawa, Japan and [3]Department of Ophthalmology, Seoul National University College of Medicine, Seoul, Korea
Correspondence: Dr N Matsumoto, Department of Human Genetics, Yokohama City University Graduate School of Medicine, Fukuura 3-9, Kanazawa-ku, Yokohama 236-0004, Japan.
E-mail: naomat@yokohama-cu.ac.jp
Received 3 October 2011; revised 6 December 2011; accepted 5 January 2012; published online 2 February 2012

heart defects in affected males, suggesting that genomic rearrangements of *NHS* are able to cause the X-linked cataract.

In this report, mutation screening and genomic microarray revealed a heterozygous mutation in *BCOR* and genomic rearrangements involving *NHS* in the three affected females of a Korean family with congenital cataract, dental abnormalities and 2nd–3rd toe syndactyly. Detailed molecular analysis will be presented.

MATERIALS AND METHODS

Clinical report

The Korean family with congenital cataract was previously described (as family 4) (Figure 1a).[12] Clinical features are summarized in Table 1. In the elder sister (MC17, the proband), bilateral congenital cataracts were noted 100 days after birth. Bilateral lensectomy and secondary intraocular lens insertion were performed. Ventricular septal defect, atrial septal defect, patent ductus arteriosus, delayed dentition, bilateral broad halluces, bilateral 2nd–3rd toe syndactyly, bilateral hammer toes and right brachyphalangia of fourth toe were also recognized. Mental development was normal. In the younger sister (MC18), bilateral congenital cataracts were also recognized. Bilateral lensectomy and secondary intraocular lens insertion were performed at ages of 2 months and 3 years, respectively. Right inguinal hernia, delayed dentition, and bilateral broad halluces, bilateral 2nd–3rd toe syndactyly, and bilateral hammer toes were noted (Figures 1b and c). She had learning difficulties at school, but IQ was not measured. In the mother (MC17b), bilateral congenital cataracts were noted and left lensectomy was performed at age of 10 years. Because of her dental anomalies and hypodontia, all her teeth were surgically removed. Bilateral 2nd–3rd toe syndactyly and bilateral hammer toes were noted. Her intelligence was normal. All the three affected members shared bilateral congenital cataracts, delayed dentition, bilateral 2nd–3rd toe syndactyly and bilateral hammer toes. Dysmorphic facial features were unseen.

DNA sequencing

Experimental protocols were approved by Institutional Review Boards for Ethical Issues at Yokohama City University School of Medicine and the Committee for the Ethical Issues on Human Genome and Gene Analysis, Seoul National University. Informed consent was obtained from all individuals. Genomic DNA was obtained from peripheral leukocytes using QIAGEN Blood and Cell Culture DNA Midi Kit (QIAGEN, Hilden, Germany). DNA was amplified using GenomiPhi V2 kit (GE healthcare, Buckinghamshire, UK). In *BCOR*, there are three isoforms: isoform a (GenBank accession number NM_017745.5), isoform b (GenBank accession number NM_001123384.1) and isoform c (GenBank accession number NM_001123385.1). In *NHS*, there are two isoforms: isoform 1 (GenBank accession number NM_198270.2) and isoform 2 (GenBank accession number NM_001136024.2). Nucleotide sequences of 1st to 15th exons of *BCOR* and 1st to 8th exons of *NHS* covering all the protein coding region as well as exon–intron borders were analyzed. Polymerase chain reaction (PCR) conditions and primer information are shown in Supplementary Table 1. PCR products were purified with ExoSAP (USB, Cleveland, OH, USA) and sequenced with BigDye terminator 3.1 (Applied Biosystems, Foster City, CA, USA) on 3100 and 3500×l Genetic Analyzer (Applied Biosystems). Sequences of patients were compared with the reference human genome sequences (based on the UCSC Genome Browser coordinate, February 2009) with Sequencher 4.10.1. (Gene Codes, Ann Arbor, MI, USA).

Copy number analysis

Copy number variations (CNVs) were investigated by Cytogenetics Whole-Genome 2.7M. Array (Affymetrix, Santa Clara, CA, USA) based on the manufacturer's instruction using 100 ng genomic DNA from three affected females (MC17b, MC17 and MC18). Copy number alterations were analyzed by Chromosome Analysis Suite (Affymetrix) with NetAffx 30.1 annotations (hg18 assembly). Any filters such as minimum size and probe numbers of CNVs were not applied. The selection criteria for putative pathogenic CNVs were as follows: (1) CNVs were shared with three affected females, (2) CNVs encompassed exons and (3) CNVs were not present in the Database of Genomic Variants (http://projects.tcag.ca/variation/).

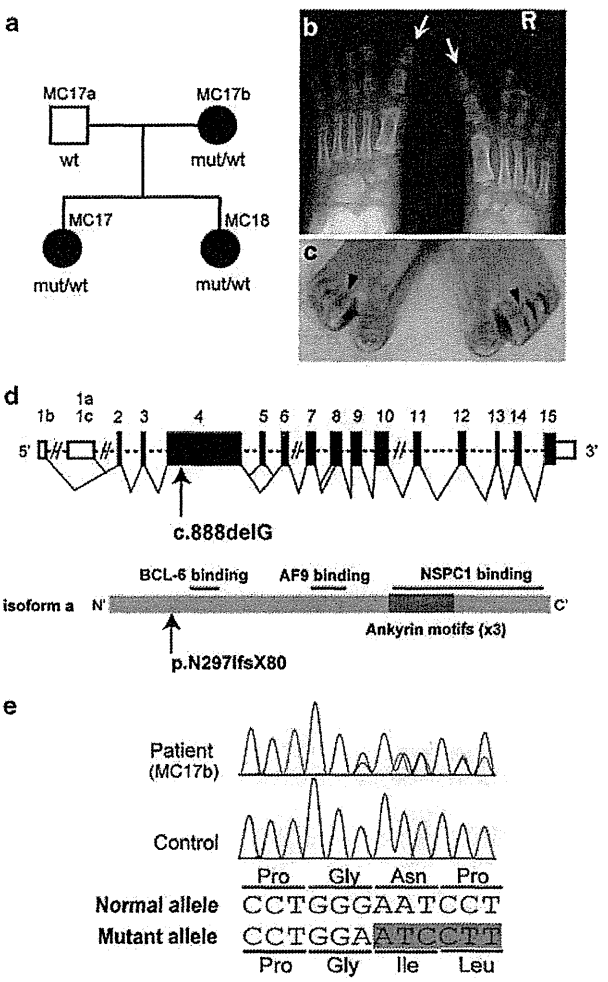

Figure 1 Pedigree, foot malformation and a *BCOR* mutation found in the family. (**a**) Familial pedigree. Black and open symbols denote affected and unaffected individuals, respectively. (**b**, **c**) Bilateral broad halluces (the big toe, arrows in **b**), bilateral 2nd–3rd cutaneous syndactyly (arrowheads in **c**) and bilateral hammer toes in MC18. (**d**) Schematic representation of the *BCOR* gene (top). UTR and coding region are open and filled rectangles, respectively. Alternative splicing by three different isoforms is shown. The isoform b is absence of exon 5 and the isoform c is 102bp and 156bp longer than the isoform a and b, respectively. The location of the c.888delG mutation is indicated by an arrow. The protein structure of BCOR (isoform a, bottom). Three consecutive ankyrin motifs are indicated as a dark-gray box. The three binding sites for BCL-6, AF9 and NSPC1 are indicated with horizontal bars. (**e**) Electropherograms showing the mutation in the affected patient (MC17b) (top) and a control (bottom). A single nucleotide deletion in exon 4 results in a frameshift. mut, a mutant allele; wt, a wild type allele.

Cloning of duplication breakpoints

DNA of the affected mother (MC17b) was digested with restriction enzymes: *Eco*RI, *Nsi*I, *Xba*I, *Bam*HI and *Bgl*II (New England Biolabs, Beverly, MA, USA). Digested DNA was self-ligated by Ligation High ver. 2 (Toyobo, Osaka, Japan), precipitated with ethanol, and dissolved in 20 µl EB buffer (QIAGEN, Tokyo, Japan). Inverse PCR was performed in 25 µl volume containing 2 µl ligated DNA, 1× PCR buffer for KOD FX, 0.4 mM each dNTPs, 0.5 µM each primer and

Table 1 Clinical features of patients with a *BCOR* mutation

	MC17b	*MC17*	*MC18*
Age	41	11	8
Sex	Female	Female	Female
Ocular features			
Congenital cataract	+	+	+
Microphthalmia/microcornea	–	–	–
Coloboma	–	–	–
Ptosis	–	–	–
Secondary glaucoma	–	+	+
Nystagmus	–	–	–
Cardiac features	–	+	–
Septal defects	–	+	–
Patent ductus arteriosus	–	+	–
Dental features			
Delayed/persistent/unerupted dentition	+	+	+
Root radiculomegaly (secondary teeth)	ND	ND	ND
Hypodontia (secondary teeth)	+	ND	ND
Duplication/fusion (secondary teeth)	ND	ND	ND
Skeletal features			
Hammer toes (camptodactyly)	+	+	+
Second–third toe syndactyly	+	+	+
Broad halluces (big toe)	–	+	+
Brachyphalangia of the fourth right toe	–	+	–
Radioulnar synostosis	ND	ND	ND
Lodosis/scoliosis/vertebral fusion	ND	ND	ND
Other features			
Mental retardation	–	–	+
Hearing impairment	–	ND	ND
Inguinal hernia	–	–	+

Abbreviation: ND, Not determined.
A plus (+) or minus (–) sign denotes the presence or absence of a particular physical feature.

0.5 U KOD FX polymerase (Toyobo). PCR were cycled 35 times at 98 °C for 10 s, 68 °C for 10 min. PCR products electrophoresed in 1% agarose gel were stained with ethidium bromide and the aberrant band was extracted using QIAEXII Gel Extraction Kit (QIAGEN, Tokyo, Japan) and sequenced. Primer information is available on request.

X inactivation study and haplotype analysis

X inactivation pattern was studied using the human androgen receptor assay and fragile X mental retardation locus methylation assay as previously described.[13–15] Briefly, genomic DNA of a patient (MC17), the parents (MC17a and MC17b), a control male and a control female was digested with two methylation-sensitive enzymes, *Hpa*II and *Hha*I. PCR was performed with human androgen receptor assay primers (FAM-labeled ARf: 5′-CCAGAAT CTGTTCCAGAGCGTGC-3′; ARr: 5′-CTCTACGATGGGCTTGGGGAGAA C-3′)[16] and fragile X mental retardation assay primers (FAM-labeled FMR1f: 5′-AGCCCCGCACTTCCACCACCAGCTCCTCCA-3′; FMR1r: 5′-GCTCAGCT CCGTTTCGGTTTCACTTCCGGT-3′). Fluorescent-labeled products were analyzed on an ABI PRISM 3100 or 3130×l Genetic analyzer and GeneMapper Software version 4.0 (Applied Biosystems). One of affected females (MC18) was not analyzed because of insufficient amount of genomic DNA. According to published criteria, X inactivation ratios of ⩽80:20 were considered random and ratios >80:20 were considered skewed and ratios >90:10 were considered highly skewed.[16,17]

X chromosome haplotype was analyzed using 12 microsatellite markers (*DXS1060, DXS8051, DXS987, DXS1226, DXS1214, DXS1068, DXS993, DXS991, DXS986, DXS8055, DXS1047* and *DXS1073*). Fluorescent- labeled (either FAM, VIC or NED) forward primers and tailed reverse primers were purchased from Applied Biosystems. These markers were based on the Marshfield genetic map (http://research.marshfieldclinic.org/genetics). PCR was cycled 40 times at 94 °C for 30 s, 55 °C for 30 s and 72 °C for 30 s in 10 μl volume containing 50 ng DNA, 1× ExTaq buffer, 0.2 mM each dNTP, 0.4 μM each primer and 0.1 U ExTaq HS polymerase. Haplotypes were manually constructed.

RESULTS

We detected a *BCOR* mutation, c. 888delG in MC17, MC17b and MC18 (Figures 1d and e). The mutation may result in insertion of 80 new amino acids after the mutation site with a premature stop codon at position 377 (p.N297IfsX80). The mutation was completely co-segregated with OFCD phenotypes in this family (Figure 1a). Sequencing of the entire *NHS* coding region detected no pathological mutations in this family.

The Cytogenetics Whole-Genome 2.7 M array detected a total of 48 CNVs (12 duplications and 36 deletions) in any of the affected females. The CNVs, which encompassed exons, were 8 duplications and 13 deletions. Among them, two duplications and one deletion were shared with three affected females. The one deletion was present in the Database of Genomic Variants. Thus, the CNVs fulfilling the criteria for pathogenic CNVs were two interstitial duplications. The 740-kb duplication at Xp22.2–22.13 encompassed exons 2–18 of *REPS2* (MIM *300317) and exons 1–3 of *NHS*. The other 110-kb duplication at Xp21.3 contained exon 2 of interleukin-1 receptor accessory protein-like 1 (*IL1RAPL1*) (MIM *300206) (Figure 2a). We were unable to examine the duplications by fluorescent *in situ* hybridization because only DNA samples were available. Instead, inverse PCR of self-ligated DNA with different sets of primers was able to amplify an expected fragment from normal *NHS* allele in all sets of primers, suggesting that the presence of one or more normal *NHS* alleles (Figures 2b and c). In addition, several attempts successfully cloned one of rearrangement junctions in relation to *NHS* (Figure 2c). This aberrant band showed that the sequences of intron 1 of *IL1RAPL1* followed the sequences of intron 3 of *NHS*, suggesting that two duplications were tandemly connected (Figure 2d, upper cases). More complicatedly, 62-bp sequences of intron 3 of *IL1RAPL1* with inverted orientation were inserted between intron 3 of *NHS* and intron 1 of *IL1RAPL1* (Figure 2d, lower cases). The other possible breakpoints, which may result in disruption of *NHS* locus could not be determined regardless of rigorous attempts. Thus there seems to be two normal *NHS* alleles and an extra *NHS* allele, in which exons 1–3 of *NHS* was connected to exon 2 of *IL1RAPL1*. Copy number of the *BCOR* gene was normal. In human androgen receptor assays, the mother (MC17b) was skewed pattern (8%), whereas the elder sister (MC17) showed a random pattern (26%). In fragile X mental retardation assays, the mother (MC17b) and elder sister (MC17) showed a highly skewed pattern (<1%) and a random pattern (48%), respectively. X-chromosome haplotype analysis was able to separate all the alleles in this family (Supplementary Figure 1). The inactivated allele in the mother harbored the *BCOR* mutation and the *NHS* rearrangement.

DISCUSSION

BCOR functions as a corepressor of BCL-6, which is a POZ/zinc finger transcription repressor.[4] BCOR have three consecutive ankyrin motifs, an AF9 (ALL1 fused gene from chromosome 9) binding site and an NSPC1 (nervous system polycomb-1) binding site.[4,18,19] Recently, the

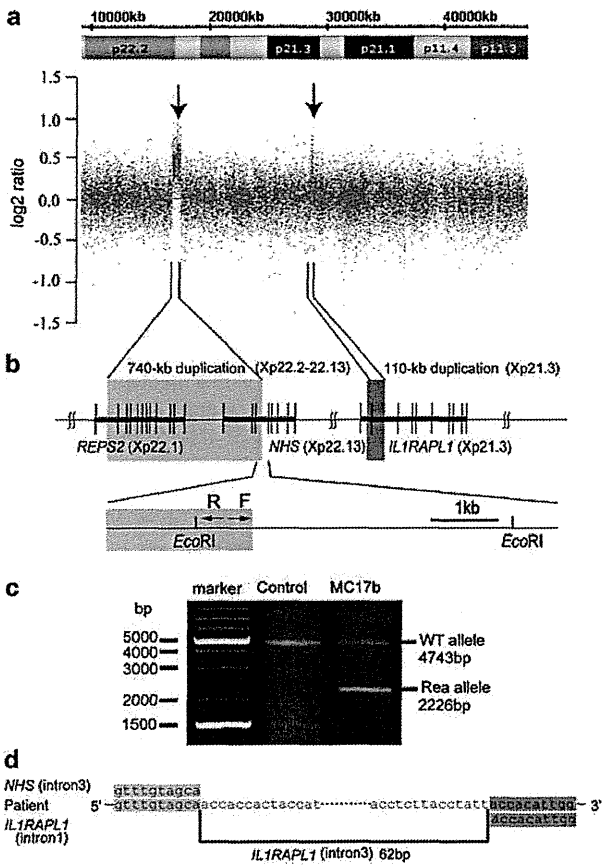

Figure 2 Two microduplications at Xp22.2–22.13 and Xp21.3. (**a**) Array profile of a part of chromosome X in the elder sister (MC17). *x* and *y* axis show the genomic location from the p telomere of chromosome X (UCSC coordinates, May, 2006) (upper) and $\log_2$ (Signal ratio) values (lower), respectively. The 740-kb duplication at Xp22.2–22.13 and the 110-kb duplication at Xp21.3 are indicated by arrows. (**b**) Upper shows schematic representation of two duplicated regions (highlighted in gray). Three genes (*REPS2*, *NHS* and *IL1RAPL1*) are oriented in the same direction (from centromere to telomere). Lower indicates scheme of inverse PCR using self-ligated DNA after digestion with *Eco*RI. Primers are shown by arrows (F, forward; R, reverse). (**c**) Gel image of inverse PCR products performed as shown in (**b**). Upper and lower bands represent wild-type allele (WT allele) and rearranged allele (Rea allele), respectively. The DNA of both bands was extracted from agarose gel and sequenced. (**d**) Sequence of a Rea allele is shown. The top, middle and bottom indicate sequences of the intron 3 of *NHS*, rearranged junction and intron 1 of *IL1RAPL1*, respectively. The 62 nucleotides of intron 3 of *IL1RAPL1* (lower cases) were inserted in an inverted orientation between intron 3 of *NHS* and intron 1 of *IL1RAPL1*. Matched sequences are highlighted with gray shadows.

minimal BCL-6 binding site was identified within residues 498–514, which is located in exon 4.[20] In this study, a novel *BCOR* mutation, c.888delG (p.N297IfsX80) in exon 4, was found in this family. We assumed the mutant transcript with this mutation may undergo nonsense-mediated mRNA decay, but we could not confirm it as no living cells were available from the patients. A total of 31 mutations in *BCOR* were registered in Human Gene Mutation Database (http://www.biobase-international.com/). All the mutations result in premature stop codons. Exon 4 harbors 40% of mutations (12/30), leading to truncated proteins lacking BCL-6, AF9 and NSPC1 binding sites, and ankyrin motifs if translated. Lack of BCL-6 binding site could not explain the OFCD phenotypes because BCL-6-deficient mice did not show ocular, dental and skeletal phenotypes.[21,22] Moreover, an OFCD mutant protein, that lacked ankyrin motifs and NSPC1 binding site, showed transcriptional repression activity similar to that of wild type.[3] Thus, the c.888delG mutation in *BCOR* may be associated with loss of *BCOR* transcripts through nonsense-mediated mRNA decay.

By genomic microarray, two microduplications were detected in MC17, MC18 and MC17b: one at Xp22.2–22.13 involving a part of *REPS2* and *NHS*, and the other at Xp21.3 containing exon 2 of *IL1RAPL1*. Previously, complex duplication-triplication rearrangements of the *NHS* gene in a family with congenital cataract were reported, suggesting that genomic rearrangements of *NHS* are able to cause the X-linked cataract.[8] This family did not show the typical features of NHS such as dental anomalies, dysmorphism and developmental delay, and congenital heart defects were diagnosed in four out of six affected males. The complex rearrangement consists of triplication embedded within a duplication region. The triplicated region includes the *NHS* genes except exon 1, and the entire *SCML1* and *RAI2* genes. Coccia *et al.*[8] described that the additional phenotype of congenital heart defects observed in some affected males could be because of perturbed *NHS* gene transcription or increased dosage of the *NHS*, *SCML1* or *RAI2* genes. In our cases, two normal *NHS* alleles may exist in addition to an extra *NHS* allele, in which exons 1–3 of *NHS* was connected to individual exon 2 of *IL1RAPL1*, keeping the protein coding frame if properly spliced. Because the transcript from the extra *NHS* allele did not have polyA signal sequences, the allele is likely to produce no functional protein. Thus, the situation was totally different between our cases and Coccia's *et al.*'s[8] cases.

Recently, Honda *et al.*[23] reported two unrelated X-linked mental retardation Japanese families, which possessed the similar duplication found in our Korean family: the 737-kb duplication at Xp22.2, which contains a part of *REPS2* and *NHS*, and the 100-kb duplication at Xp21.3, which contains a part of *IL1RAPL1*. In their report, fluorescent *in situ* hybridization analysis revealed that the clone RP11-438J7, which entirely covered the duplication at Xp21.3, demonstrated two distinct signals at Xp in metaphases, suggesting that the duplication at Xp21.3 was inserted separately from the original site. The clone RP11-2K15 at Xp22.2, spanning the breakpoint of *REPS2*, showed one bright strong signal, suggesting that the duplication at Xp22.2 occurred in the proximity. Interestingly, the one of two signals of the RP11-438J7 was close to that of RP11-2K15 at Xp22.2, suggesting that the duplication involving *IL1RAPL1* was inserted at Xp22.2. Their result is consistent with our data of the duplication breakpoint, in which the breakpoint in *NHS* was connected with the breakpoint of *IL1RAPL1*. Based on our experiences, high-density array experiments of >500 Japanese cases never showed such the genomic rearrangement involving *NHS*, implying that the rearrangement is very rare in Japanese population. It is noteworthy that congenital cataract and dental abnormalities were not pointed out in all the members (males and carrier females).[23] Thus, it is unlikely that the genomic rearrangement involving *NHS* causes congenital cataract and dental abnormalities as found in our family.

IL1RAPL1 is a causative gene for X-linked mental retardation,[24] and the microduplication at Xp21.3 containing exon 2 of *IL1RAPL1* was suggested to cause MR in affected males.[23] Most carrier females of *IL1RAPL1* mutations and the carrier mother of the microduplication involving *IL1RAPL1* showed normal intelligence.[23–25] In this study, one of the three affected females (MC18) had learning difficulties at school, which could be mild presentation of MR. As 18% of patients with *BCOR* mutations showed MR,[6] it is reasonable that the *BCOR* mutation, rather than *IL1RAPL1* rearrangement, causes mild MR in MC18.

Skewed and random X-inactivation in the mother (MC17b) and the elder daughter (MC17) was confirmed, respectively, in this family. In OFCD, skewed X-inactivation with the preferential inactivation of the mutated allele were recognized in eight affected females (like the mother, MC17b), suggesting that the *BCOR* mutations may lead to a selective disadvantage in blood leukocytes.[3,26] However, it has been reported that the X-inactivation pattern in blood leukocytes are unable to determine the severity of disease phenotypes as X-inactivation pattern may vary among tissues.[27] We suspect that X-inactivation pattern is different between peripheral blood leukocytes and respective tissues associated with OFCD phenotype.

In conclusion, a new OFCD family is described with a novel *BCOR* mutation. Clinical features overlap between OFCD and NHS, both of which belong to a spectrum of X-linked microphthalmia disorders.[6] Our cases have a *BCOR* mutation and genomic rearrangements involving *NHS*, confusing us to address the genetic etiology in the family. However, the presence of bilateral 2nd–3rd toe syndactyly and septal heart defects, which is unique to OFCD, can lead us to the conclusion that the *BCOR* mutation is the major determinant for the phenotypes in this family. Careful examination of associated anomalies will be useful for genetic testing of X-linked microphthalmia disorders.

ACKNOWLEDGEMENTS

We thank the family members for their participation in this study. This work was supported by Research Grants from the Ministry of Health, Labour and Welfare (HS, N Miyake and N Matsumoto) and the Japan Science and Technology Agency (N Matsumoto) and Grant-in-Aid for Scientific Research from Japan Society for the Promotion of Science (N Matsumoto).

Web Resources

The URLs for data presented herein are as follows: UCSC Genome Browser, http://genome.ucsc.edu/cgi-bin/hgGateway

1 Wilkie, A. O., Taylor, D., Scambler, P. J. & Baraitser, M. Congenital cataract, microphthalmia and septal heart defect in two generations: a new syndrome? *Clin. Dysmorphol.* **2,** 114–119 (1993).
2 Aalfs, C. M., Oosterwijk, J. C., van Schooneveld, M. J., Begeman, C. J., Wabeke, K. B. & Hennekam, R. C. Cataracts, radiculomegaly, septal heart defects and hearing loss in two unrelated adult females with normal intelligence and similar facial appearance: confirmation of a syndrome? *Clin. Dysmorphol.* **5,** 93–103 (1996).
3 Ng, D., Thakker, N., Corcoran, C. M., Donnai, D., Perveen, R., Schneider, A. *et al.* Oculofaciocardiodental and Lenz microphthalmia syndromes result from distinct classes of mutations in *BCOR*. *Nat. Genet.* **36,** 411–416 (2004).
4 Huynh, K. D., Fischle, W., Verdin, E. & Bardwell, V. J. BCoR, a novel corepressor involved in BCL-6 repression. *Genes Dev.* **14,** 1810–1823 (2000).
5 Wamstad, J. A. & Bardwell, V. J. Characterization of *Bcor* expression in mouse development. *Gene Expr. Patterns* **7,** 550–557 (2007).
6 Hilton, E., Johnston, J., Whalen, S., Okamoto, N., Hatsukawa, Y., Nishio, J. *et al. BCOR* analysis in patients with OFCD and Lenz microphthalmia syndromes, mental retardation with ocular anomalies, and cardiac laterality defects. *Eur. J. Hum. Genet.* **17,** 1325–1335 (2009).
7 Nance, W. E., Warburg, M., Bixler, D. & Helveston, E. M. Congenital X-linked cataract, dental anomalies and brachymetacarpalia. *Birth Defects Orig. Artic. Ser.* **10,** 285–291 (1974).
8 Coccia, M., Brooks, S. P., Webb, T. R., Christodoulou, K., Wozniak, I. O., Murday, V. *et al.* X-linked cataract and Nance-Horan syndrome are allelic disorders. *Hum. Mol. Genet.* **18,** 2643–2655 (2009).
9 Lewis, R. A., Nussbaum, R. L. & Stambolian, D. Mapping X-linked ophthalmic diseases. IV. Provisional assignment of the locus for X-linked congenital cataracts and microcornea (the Nance-Horan syndrome) to Xp22.2-p22.3. *Ophthalmology.* **97,** 110–120; discussion 120–111 (1990).
10 Stambolian, D., Lewis, R. A., Buetow, K., Bond, A. & Nussbaum, R. Nance-Horan syndrome: localization within the region Xp21.1-Xp22.3 by linkage analysis. *Am. J. Hum. Genet.* **47,** 13–19 (1990).
11 Burdon, K. P., McKay, J. D., Sale, M. M., Russell-Eggitt, I. M., Mackey, D. A., Wirth, M. G. *et al.* Mutations in a novel gene, *NHS*, cause the pleiotropic effects of Nance-Horan syndrome, including severe congenital cataract, dental anomalies, and mental retardation. *Am. J. Hum. Genet.* **73,** 1120–1130 (2003).
12 Miyamoto, T., Yu, Y. S., Sato, H., Hayashi, H., Sakugawa, N., Ishikawa, M. *et al.* Mutational analysis of the human *MBX* gene in four Korean families demonstrating microphthalmia with congenital cataract. *Turk J. Pediatr.* **49,** 334–336 (2007).
13 Allen, R. C., Zoghbi, H. Y., Moseley, A. B., Rosenblatt, H. M. & Belmont, J. W. Methylation of *Hpa*II and *Hha*I sites near the polymorphic CAG repeat in the human androgen-receptor gene correlates with X chromosome inactivation. *Am. J. Hum. Genet.* **51,** 1229–1239 (1992).
14 Carrel, L. & Willard, H. F. An assay for X inactivation based on differential methylation at the fragile X locus, *FMR1*. *Am. J. Med. Genet.* **64,** 27–30 (1996).
15 Nishimura-Tadaki, A., Wada, T., Bano, G., Gough, K., Warner, J., Kosho, T. *et al.* Breakpoint determination of X; autosome balanced translocations in four patients with premature ovarian failure. *J. Hum. Genet.* **56,** 156–160 (2011).
16 Kubota, T., Nonoyama, S., Tonoki, H., Masuno, M., Imaizumi, K., Kojima, M. *et al.* A new assay for the analysis of X-chromosome inactivation based on methylation-specific PCR. *Hum. Genet.* **104,** 49–55 (1999).
17 Amos-Landgraf, J. M., Cottle, A., Plenge, R. M., Friez, M., Schwartz, C. E., Longshore, J. *et al.* X chromosome-inactivation patterns of 1,005 phenotypically unaffected females. *Am. J. Hum. Genet.* **79,** 493–499 (2006).
18 Srinivasan, R. S., de Erkenez, A. C. & Hemenway, C. S. The mixed lineage leukemia fusion partner AF9 binds specific isoforms of the BCL-6 corepressor. *Oncogene* **22,** 3395–3406 (2003).
19 Gearhart, M. D., Corcoran, C. M., Wamstad, J. A. & Bardwell, V. J. Polycomb group and SCF ubiquitin ligases are found in a novel BCOR complex that is recruited to BCL6 targets. *Mol. Cell Biol.* **26,** 6880–6889 (2006).
20 Ghetu, A. F., Corcoran, C. M., Cerchietti, L., Bardwell, V. J., Melnick, A. & Prive, G. G. Structure of a BCOR corepressor peptide in complex with the BCL6 BTB domain dimer. *Mol. Cell.* **29,** 384–391 (2008).
21 Ye, B. H., Cattoretti, G., Shen, Q., Zhang, J., Hawe, N., de Waard, R. *et al.* The *BCL-6* proto-oncogene controls germinal-centre formation and Th2-type inflammation. *Nat. Genet.* **16,** 161–170 (1997).
22 Dent, A. L., Shaffer, A. L., Yu, X., Allman, D. & Staudt, L. M. Control of inflammation, cytokine expression, and germinal center formation by BCL-6. *Science* **276,** 589–592 (1997).
23 Honda, S., Hayashi, S., Imoto, I., Toyama, J., Okazawa, H., Nakagawa, E. *et al.* Copy-number variations on the X chromosome in Japanese patients with mental retardation detected by array-based comparative genomic hybridization analysis. *J. Hum. Genet.* **55,** 590–599 (2010).
24 Carrie, A., Jun, L., Bienvenu, T., Vinet, M. C., McDonell, N., Couvert, P. *et al.* A new member of the IL-1 receptor family highly expressed in hippocampus and involved in X-linked mental retardation. *Nat. Genet.* **23,** 25–31 (1999).
25 Nawara, M., Klapecki, J., Borg, K., Jurek, M., Moreno, S., Tryfon, J. *et al.* Novel mutation of *IL1RAPL1* gene in a nonspecific X-linked mental retardation (MRX) family. *Am. J. Med. Genet. A* **146A,** 3167–3172 (2008).
26 Hedera, P. & Gorski, J. L. Oculo-facio-cardio-dental syndrome: skewed X chromosome inactivation in mother and daughter suggest X-linked dominant Inheritance. *Am. J. Med. Genet. A* **123A,** 261–266 (2003).
27 Bartnik, M., Derwinska, K., Gos, M., Obersztyn, E., Kolodziejska, K. E., Erez, A. *et al.* Early-onset seizures due to mosaic exonic deletions of *CDKL5* in a male and two females. *Genet. Med.* **13,** 447–452 (2011).

Supplementary Information accompanies the paper on Journal of Human Genetics website (http://www.nature.com/jhg)

CLINICAL GENETICS An International Journal of Genetics, Molecular and Personalized Medicine

Clin Genet 2012: 81: 399–402
Printed in Singapore. All rights reserved

CLINICAL GENETICS
doi: 10.1111/j.1399-0004.2011.01733.x

Letter to the Editor

Association of genomic deletions in the *STXBP1* gene with Ohtahara syndrome

To the Editor:

Ohtahara syndrome (OS) is characterized by early-onset of seizures, suppression-burst patterns on electroencephalogram (EEG), and severe psychomotor retardation (1–3). *De novo* mutations in the *STXBP1* gene, including various point mutations and one complete deletion, have been found in about one-third of Japanese cases of cryptogenic OS (4–6). However, the clinical spectrum of *STXBP1* mutations can be applied to other pathologies. For instance, in one study, *STXBP1* abnormalities including a microdeletion were detected in approximately 10% of patients (5/49) with early-onset epileptic encephalopathy that did not fit into a specific epilepsy syndrome (7). Other studies have also detected *de novo STXBP1* mutations in 2 of 95 individuals with mental retardation and non-syndromic epilepsy (8), in addition to the detection of a *de novo* partial deletion in a child with epilepsy and autistic features (9, 10). On the basis of these findings, extensive genetic testing including copy number analysis of *STXBP1* should be considered in children with early-onset seizures. However, the use of high-resolution copy number analysis of *STXBP1* thus far has been limited.

In this study, we performed customized array comparative genomic hybridization (aCGH) analysis, in which a total of 27,026 probes covering the *STXBP1* locus (UCSC coordinates, May 2006: Chr9: 129,350,808–129,558,072 bp) were distributed with 5-bp spacing except for repeating element regions (Roche NimbleGen, Tokyo, Japan). Among the 28 patients with cryptogenic OS tested, we found pathogenic *de novo* deletions in two patients (7.1%), where one 4.6-kb deletion included only exon 4, and the other 2.85-Mb one involved the entire *STXBP1* gene (Table 1).

Patient 1506, a product of unrelated healthy parents, had no problems in the perinatal period. Tonic seizures with a flexion of the upper extremities started at 32 days of age, and frequent myoclonic seizures subsequently appeared. On the basis of suppression-burst pattern on EEG, the patient was diagnosed as having OS or early myoclonic encephalopathy (EME), which is another epileptic syndrome showing suppression-burst pattern on EEG (11). As OS and EME have common features, they can be difficult to distinguish (2, 3). Brain magnetic resonance imaging (MRI) revealed normal neuroanatomy. High-dose phenobarbital was able to effectively reduce the frequency of seizures. Customized aCGH and breakpoint polymerase chain reaction (PCR) analyses detected a *de novo* 4635-bp deletion involving exon 4 of the *STXBP1* gene (Fig. 1a–c). The presence of a 2-bp microhomology at the deletion junction suggested non-homologous recombination leading to a

Table 1. Copy number alterations found in OS patients

	Findings of customized aCGH and 2.7M array (upper)/sequence-confirmed rearrangements (lower)						
Patient	Aberrations	Start (bp)	End (bp)	Size (bp)	Genes	Inheritance	Origin
1506	Deletion	129,457,591	129,462,084	4493	*STXBP1*(Ex4)	*De novo*	Unknown[a]
		129,457,463	129,462,098	4635	–	–	–
2231	Deletion	129,020,847	131,869,806	2,848,959	70 RefSeq genes including *STXBP* and *SPTAN1*	*De novo*	Paternal[b]
		129,020,309	131,870,400	2,850,091		–	–

aCGH, array comparative genomic hybridization; OS, Ohtahara syndrome.
[a]No informative markers were available within the 4.6-kb region corresponding to the deletion.
[b]Examined by the *D9S918* (UCSC coordinates, May 2006: Chr9: 129,497,050–129,497,376 bp) microsatellite marker.

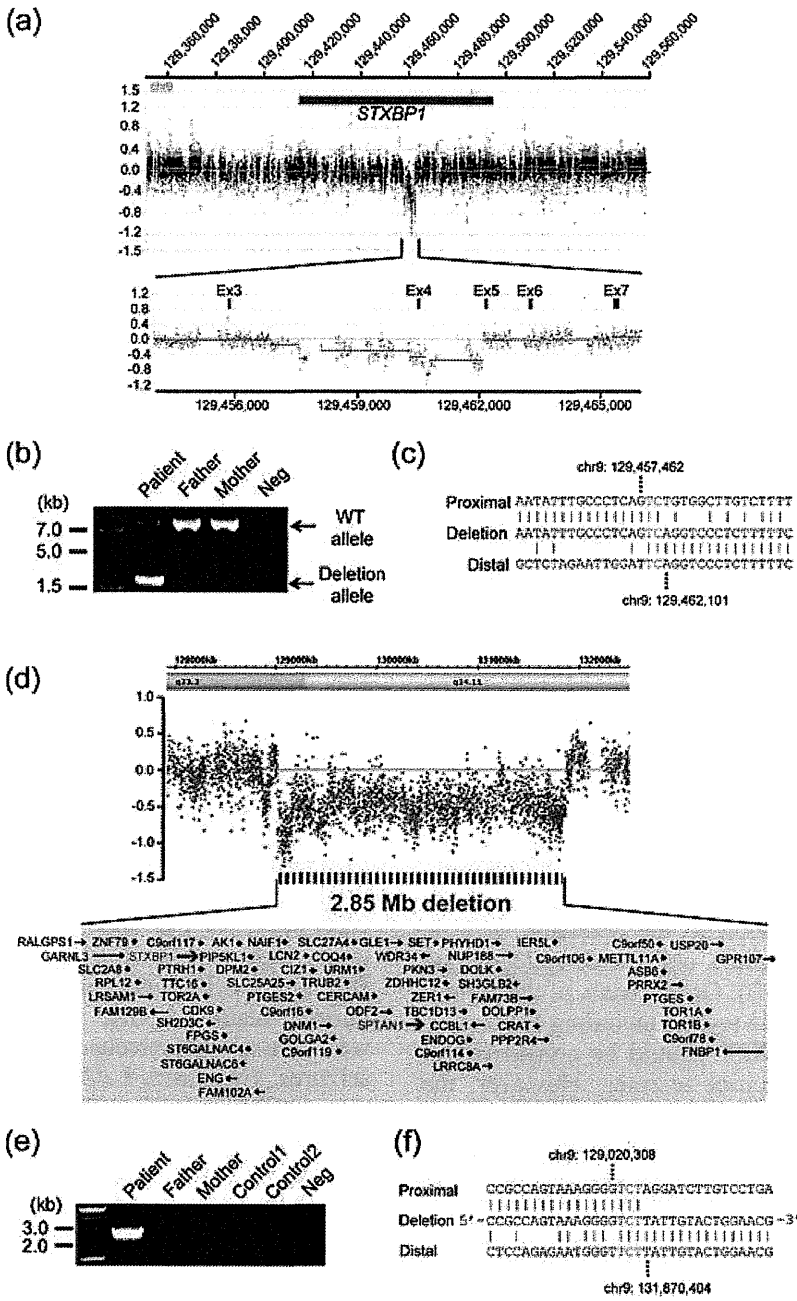

Fig. 1. The detection of two microdeletions using microarray. (**a**) A customized array comparative genomic hybridization (aCGH) profile of *STXBP1* locus in patient 1506. *x*- and *y*-axis show the genomic location from the p telomere of chromosome 9 (UCSC coordinates, May, 2006) and $\log_2$ (Cy3/Cy5 signal ratio) values (green dots ≥ 0.25; $-0.25 <$ black dots < 0.25; red dots ≤ -0.25), respectively (top panel). A close up view of the aCGH profile along with maps of the *STXBP1* exons (blue rectangles), showing the deletion of exon 4 (bottom panel). (**b**) Polymerase chain reaction (PCR) analysis of the family of patient 1506. Primers flanking the deletion amplified both 6398- and 1763-bp products from the wild type and deletion alleles, respectively, of the patient. However, the patient's parents had only a 6398-bp product, indicating the presence of a *de novo* deletion (Neg, negative control which contained no template DNA). (**c**) The deletion junction sequence. The top, middle and bottom strands show the proximal, deleted, and distal sequences, respectively. The two overlapping nucleotides are colored in red. (**d**) The 2.7M array profile clearly showed a 2.85-Mb deletion at 9q33.3-34.11 found in patient 2231 (top panel). A total of 70 RefSeq genes, including *STXBP1* and *SPTAN1*, were mapped within the deletion (bottom panel). (**e**) The breakpoint PCR analysis of the family of patient 2231. Primers flanking the deletion successfully amplified a 2430-bp product from the patient, indicating that the deletion occurred *de novo* (Neg, negative control that contained no template DNA). (**f**) The deletion junction sequence. The top, middle and bottom strands show the proximal, deleted and distal sequences, respectively. The three overlapping nucleotides are colored in red. The PCR conditions and primer sequences are available on request.

rearrangement (Fig. 1c) (12). The deletion of exon 4 was also confirmed by reverse transcriptase-PCR (Fig. S1, Supporting Information).

Patient 2231 was born at term after *in vitro* fertilization and embryo transfer. The body weight at birth was 2134 g (−2.4 SD), height 44.5 cm (−2.3 SD), and head circumference 32.0 cm (−0.8 SD). Multiple anomalies including cleft lip and palate, ventricular septal defect, overlapping fingers, and small penis were noted. G-banded chromosomal analysis was normal. The patient had an onset of sudden crying at 1 week of age followed by a cluster of epileptic spasms with suppression-burst pattern on EEG at 1 month. A brain MRI at 2 months showed a thin corpus callosum and relatively small cerebellum. After treatment with antiepileptic drugs proved ineffective, a ketogenic diet reduced the frequency of seizures. At 19 months, he showed spastic quadriplegia and profound intellectual disability at the level of a 2-month old. Customized aCGH, subsequent whole-genome 2.7M Array (Affymetrix, Santa Clara, CA), and breakpoint PCR analyses found a *de novo* 2.85-Mb microdeletion including *STXBP1* and *SPTAN1* (13) (Fig. 1d–f). The presence of a 3-bp homology at the deletion junction further suggested non-homologous recombination leading to the rearrangement (Fig. 1f).

In conclusion, our high-resolution copy number analysis in *STXBP1* locus revealed a 4.6-kb deletion encompassing only exon 4, which strongly suggests that copy number analysis covering all *STXBP1* exons should be recommended as a genetic test for children with early-onset seizures.

Supporting Information

The following Supporting information is available for this article:

Fig. S1. Examination of the mutated transcripts in lymphoblastoid cell lines derived from the patient 1506. (**a**) Reverse transcriptase polymerase chain reaction (RT-PCR) analysis of the patient with an exon 4 deletion relative to a normal control. A schematic representation of the transcript from exons 3 to 6 of *STXBP1* is indicated (top). The exons and primers are depicted as boxes and arrows, respectively. Two PCR products were amplified from the patient's cDNA: the upper was a wild-type (WT) transcript and the lower was the deleted mutant (middle). Only a single WT amplicon was detected in the control. The mutant amplicon was significantly increased by 30 μM cycloheximide (CHX) treatment for 4 h compared to dimethyl sulfoxide treatment as a vehicle control. RT (+): with reverse transcriptase, RT (−): without reverse transcriptase as a negative control. The sequence of the smaller amplicon clearly demonstrated exon 4 deletion (bottom). (**b**) Quantitative analysis of the nonsense-mediated mRNA decay (NMD) inhibition by CHX based on the data shown in (**a**). *p = 0.0023 by unpaired two tailed Student's *t*-test. Averages of duplicated experiments using two distinctive RNA samples are shown with error bars (SD). The mutant transcript lacking exon 4 created a premature stop codon at position 64, and suffered from degradation by NMD in the patient's lymphoblastoid cells. PCR conditions and the primer sequences are available on request.

Additional Supporting information may be found in the online version of this article.

Please note: Wiley-Blackwell Publishing is not responsible for the content or functionality of any supplementary materials supplied by the authors. Any queries (other than missing material) should be directed to the corresponding author for the article.

Acknowledgements

We would like to thank the patients and their families for their participation in this study. This work was supported by Research Grants from the Ministry of Health, Labour and Welfare (H. S., M. K., N. M. and N. M.), a Grant-in-Aid for Scientific Research from the Japan Society for the Promotion of Science (M. K. and N. M.), a Grant-in-Aid for Young Scientist from Japan Society for the Promotion of Science (H. S.), Research Promotion Fund from Yokohama Foundation for Advancement of Medical Science (H. S.), Research Grants from the Japan Epilepsy Research Foundation (H. S. and M. K.), and a Research Grant from Naito Foundation (N. M.).

H Saitsu[a]* *M Kato*[b]* *M Shimono*[c] *A Senju*[d] *S Tanabe*[d] *T Kimura*[d] *K Nishiyama*[a] *Y Yoneda*[a] *Y Kondo*[a] *Y Tsurusaki*[a] *H Doi*[a] *N Miyake*[a] *K Hayasaka*[b] *N Matsumoto*[a]

[a]Department of Human Genetics, Yokohama City University Graduate School of Medicine, Yokohama, Japan,

[b]Department of Pediatrics, Yamagata University Faculty of Medicine, Yamagata, Japan,

[c]Department of Pediatrics, School of Medicine, University of Occupational and Environmental Health, Kitakyushu, Japan, and

[d]Department of Pediatrics, Nihonkai General Hospital, Sakata, Japan

*These two authors contributed equally to this work.

References

1. Ohtahara S, Ishida T, Oka E et al. On the specific age dependent epileptic syndrome: the early-infantile epileptic encephalopathy with suppression-burst. No to Hattatsu 1976: 8: 270–279.
2. Djukic A, Lado FA, Shinnar S, Moshe SL. Are early myoclonic encephalopathy (EME) and the Ohtahara syndrome (EIEE) independent of each other? Epilepsy Res 2006: 70 (Suppl. 1): S68–S76.
3. Ohtahara S, Yamatogi Y. Ohtahara syndrome: with special reference to its developmental aspects for differentiating from early myoclonic encephalopathy. Epilepsy Res 2006: 70 (Suppl. 1): S58–S67.
4. Saitsu H, Kato M, Mizuguchi T et al. *De novo* mutations in the gene encoding STXBP1 (MUNC18-1) cause early infantile epileptic encephalopathy. Nat Genet 2008: 40: 782–788.
5. Saitsu H, Kato M, Okada I et al. *STXBP1* mutations in early infantile epileptic encephalopathy with suppression-burst pattern. Epilepsia 2010: 51: 2397–2405.
6. Saitsu H, Hoshino H, Kato M et al. Paternal mosaicism of an *STXBP1* mutation in OS. Clin Genet 2010. Epub ahead of print. DOI: 10.1111/j.1399-0004.2010.01575.x.